

Granular contact force density of states and entropy in a modified Edwards ensemble

Philip T. Metzger*

The KSC Applied Physics Laboratory, The John F. Kennedy Space Center, NASA
 YA-C3-E, Kennedy Space Center, Florida 32899

(Dated: February 8, 2020)

The granular contact force probability density functions (PDFs) are obtained from first principles in an ensemble analysis. The results are in excellent agreement with the experimental and simulation data. The derivation assumes Edwards’ flat measure, a density of states (DOS) that is uniform within the metastable regions of phase space. The enabling assumption, supported by physical arguments and empirical evidence, is that correlative information is not significantly recursive. Maximizing a state-counting entropy results in a transport equation that can be solved numerically. For the present this has been done using the “Mean Structure Approximation,” projecting the DOS across all angular coordinates to more clearly identify its predominant non-uniformities. These features are: (1) the Grain Factor $\bar{\Psi}$ related to grain stability and strong correlation between the contact forces on the same grain, and (2) the Structure Factor $\bar{\Upsilon}$ related to Newton’s third law and strong correlation between neighboring grains. It is argued that this frictionless case is the more fundamental one to elucidate the organization of granular packings.

PACS numbers: 45.70.Cc, 05.20.Gg, 05.10.Ln, 05.65.+b

I. INTRODUCTION

A. Deriving the Contact Force Distribution

There have been several attempts to derive the granular contact force probability density function (PDF) for static granular packings, $P_F(F)$, by using analogies from the thermal statistical mechanics [1, 2, 3, 4]. The interest arises in part because the empirical $P_F(F)$ [5, 6, 7, 8, 9, 10, 11, 12, 13, 14, 15, 16, 17, 18] has an exponential tail, reminiscent of the momentum and energy distributions of thermal systems. This implies that in some sense it is maximally entropic, that a statistical relaxation has occurred despite the fact that static packings are not thermal and have a relatively small particle count. The overall form of $P_F(F)$ is not found in thermal systems, generally having a peak or plateau near the average force and a non-zero value at zero force as illustrated in Fig. (1). These features have been observed experimentally with frictional grains [6, 7] and with frictionless emulsions [19], and in numerical simulations with frictional grains [5, 8, 11, 12, 13, 14] or purely frictionless grains [10, 15, 16, 17], and in molecular dynamics using Lennard-Jones potentials quenched beneath the glass transition [9], and in adaptive network simulations [20]. The variety of models and conditions shows that the PDF’s features are not associated with a specific type of model or the (non)existence of friction, but arise from the fundamental physics of a non-cohesive, static granular packing. Just as the density of states (DOS) for ideal Bose and Fermi gases are organized differently than the classical dilute gas and produce their own unique energy distributions, so the DOS of granular packings must

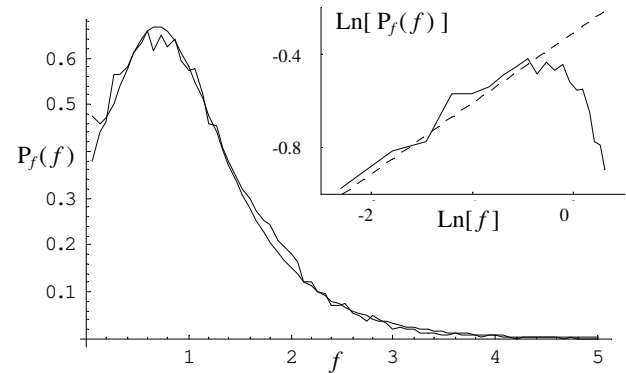


FIG. 1: Linear plot of the PDF $P_f(f)$ of the normalized vector magnitudes of the granular contact forces resulting from Monte Carlo solution of the Mean Structure Transport Equation. It has a non-zero probability density for zero force, a peak just below $f = 1$, and an exponential tail with decay constant $\beta = 1.6$. The smooth curve is a fit to Eq. (61). The log-log inset shows the behavior below $f = 1$. The dashed line is a power law of exponent $\alpha = 0.3$. These features are consistent with experimental and simulation data.

be organized in some unique way to produce this distinctive PDF. Its explanation may therefore lie in another generalization of statistical mechanics.

Such a generalization has been taking shape [21, 22], beginning with Edwards’ hypothesis [23] that all metastable packings are equally probable in the statistical ensemble, known as Edwards’ flat measure. Another line of progress is based on the concept of directed force chain networks [24], while others aim to understand the distribution of forces beneath a localized perturbation or more generally the stress response function [25], and the phenomena related to jamming and unjamming [26, 27]. This paper focuses more narrowly upon those models or hypotheses which predict a PDF by making assumptions

*Electronic address: Philip.T.Metzger@nasa.gov

about the DOS in the ensemble, including those models which take a random walk in an assumed phase space (e.g., the q model) or in a PDF space (i.e., the Boltzmann transport equation variety), and those which directly assume the form of an entropy or other thermodynamic functional. These are of interest here because they are immediately testable against the empirical PDF data and because they are directly comparable to the DOS that was assumed in Edwards' hypothesis.

Random walk models include the q model [28, 29], because the set of forces in each layer of the lattice describe a locus in the phase space while the random redistribution of those forces from one layer to the next (controlled by the stochastic q variables) represents a random walk through that space. This introduced a new way to think about granular media: the statistical relaxation does not occur dynamically through the time dimension as it does in thermal systems; rather it is a necessary feature of the *internal*, layer-by-layer static equilibrium relationships, where the spatial dimensions play the role of the time for each corresponding set of Cartesian components of force. This produces a PDF having the exponential tail. The PDF is monotonically decreasing, but it should be noted that the forces in the q model are the vertical Cartesian components of the contact forces, not the contact force magnitudes. There exists a conversion [30] between the Cartesian component PDF, $P_X(F_x)$, and the contact force magnitude PDF, $P_F(F)$, and it can be shown using this transform that the $P_F(F)$ resulting from certain q distributions will demonstrate all the correct features including the peak or plateau and the finite $P_F(0) > 0$. The main problem with the q model is simply that it does not include the physics to predict the q distribution. Several generalizations of the q model and other lattice-based models have been developed [22, 31, 32, 33]. Some of these are similarly random walks in a non-dynamic phase space, but others include explicitly dynamic features to recursively achieve organization in the percolating force network. In a future publication it will be explained why non-dynamic lattice-based models cannot achieve the organization needed to predict the PDF. This paper will lay the groundwork for that explanation.

Other models that make direct assumptions about the DOS include a Boltzmann type equation presented by Edwards and Grinev [2, 19]. It is analytically solvable and produces a $P_F(F)$ that has a peak and exponential tail. However, it predicts $P_F(F) \rightarrow 0$ as $F \rightarrow 0$, contradicting the empirical data. Several entropy maximization or functional minimization concepts have also been proposed [1, 3, 4], and these produce elements of the PDF but not all of its features as discussed in App. A.

This paper analyzes the DOS in a modified version of the Edwards ensemble [23]. The dynamical behaviors of granular media have been completely avoided so that Edwards' hypothesis alone shapes the DOS, and this is analogous to the avoidance of molecular dynamics in a pure, statistical mechanics theory. It is found that the DOS is highly self-organized and very sparse. Its form

depends upon the form of $P_F(F)$ and *vice versa* so that recursion is necessary to solve for either. Maximizing a state counting entropy in this phase space produces the recursion equation which is analogous to the Boltzmann transport equation. To elucidate the organization of the DOS, it is projected across all angular coordinates before solving numerically. The results demonstrate the success of Edwards' hypothesis in that it predicts the correct forms of the PDFs.

The success of this analysis supports the growing conviction that granular phenomena should be explainable within the purview of a generalized statistical mechanics. It also thereby identifies the essential organizing principles in static granular packings and provides an explanation why other analytical methods have not worked: in most cases the implied DOS is too uniform, not being constrained onto the surfaces where every grain is individually stable and where neighboring grains satisfy Newton's third law. These simple constraints require the packing to achieve an extremely high degree of organization before its dynamics will cease, and this produces the very sparsely distributed DOS that shapes the PDF.

B. The Form of the Contact Force Distribution

There is some variability in the form of $P_F(F)$ depending upon the conditions of the packing. It has been suggested theoretically [33] and demonstrated empirically [4, 33, 34] that with increasing stress (and therefore increasing grain deformation) the tail may evolve from an exponential form $\sim \exp(-\beta f)$ to a more rapidly decaying form such as a compressed exponential $\sim \exp(-\beta f^\alpha)$ with $\alpha > 1$, or perhaps a Gaussian ($\alpha = 2$), although this result has not been observed in all cases [7].

Also the degree of stress and fabric anisotropy during biaxial shearing has been shown to affect the PDF in the region of weak forces, causing it to evolve from having a peak to having a plateau to being a monotonically decreasing function with only a sudden change of slope near the average value of force [5, 17]; further shearing then reverses the evolution part way until it has a small peak again [5]. Some numerical simulations of frictional grains have seen peaks and others have seen plateaus, but the stress and fabric anisotropies are not usually reported.

The formation of a peak has also been connected to the jamming transition as kinetic energy is removed [9] while the packing fraction is sufficiently large [10]. Friction also affects somewhat the shape of $P_F(F)$ in the region of weak forces [14], and it is probable that this effect is history-dependent due to the hyperstaticity of frictional packings.

This analysis is concerned with the idealized case with rigid, completely static, frictionless grains, and the subsequent numerical results focus specifically on isotropic conditions. The weight of the evidence indicates that in these idealizations the tail should be exponential and the PDF should have a small peak. The expected features of

the PDF are discussed in more detail in App. A.

C. Overview

In this paper, Sec. II analyzes the DOS in the modified Edwards ensemble and develops the transport equation, including a simplified version (projected across the angle coordinates) using the Mean Structure Approximation. Sec. III presents the numerical solution of the Mean Structure Transport Equation. Sec. IV discusses the validity and relevance of the approach and identifies the essential organizational principles of static granular physics. Sec. V summarizes the findings and points to several unanswered problems and several generalizations that are needed.

II. MODIFIED EDWARDS ENSEMBLE ANALYSIS

A. Description of the Particular Ensemble

The original paper in which Edwards' hypothesis was presented was concerned with powders—which are frictional—and for the sake of clarity avoided the complications of anisotropic compaction [23]. Subsequent studies have often relied upon the influence of gravity as the source of stress, and the packings are made to explore the phase space by tapping the container [35]. This ensemble will be generalized in two ways and idealized in several other ways.

1. Generalizations of the Ensemble

First, to eliminate an unnecessary asymmetry from the packings and to render the organizational features of the physics more clear, the source of stress in these packings will be a mechanical application of force at the boundaries. There will be no body forces such as gravity. As a result, the sum of the forces perpendicular to any cross-sectional sample of grains that spans the packing will be conserved layer-by-layer for any progression of layers at the fixed orientation. The use of externally-applied stresses also allows for more generalized stress states and contact geometry fabrics than what occur in packings under the influence of gravity alone.

Second, when anisotropic stress states are applied, then anisotropic compaction may occur. This cannot be ignored because the form of $P_F(F)$ is known to evolve with that anisotropy. Therefore a more general descriptor of the internal state of the packing is needed in place of scalar compaction. The fabric tensor \mathbf{F} or the probability distribution $P_\theta(\theta)$ are the most common descriptors of fabric. However, this study will use a more informative joint probability density function (JPDF) $P_{4\theta}(\theta_1, \dots, \theta_4)$ studied in Ref.36 to correlate the contact angles that

share the same grain. This can be collapsed to $P_\theta(\theta)$,

$$P_\theta(\theta) = \frac{1}{4} \sum_{j=1}^4 \iiint \int_0^{2\pi} d^4\theta J_{4\theta}(\theta_1, \dots, \theta_4) \delta(\theta - \theta_j). \quad (1)$$

The use of the JPDF is deemed necessary because the physics of fragile media are grain-centered and the intra-grain correlations turn out to be the heart of the statistical physics, as shall be shown here. This JPDF is not completely sufficient, however, because it tells nothing of the number and size of voids created by the arrangement of neighboring grain configurations, which is an important aspect of Edwards' hypothesis and its ability to predict the evolution of scalar compaction. For the present study, the voids will be quantified simply by assuming a number of grains per unit distance in a cross-section of the 2D packing in each orthogonal direction. These quantities along with the JPDF will be specified in the ensemble rather than predicted. Evolution of the internal state of the packing is beyond the present study.

These generalizations are necessary because there are as many independent force conservation laws as there are spatial dimensions of the packing, and each conservation of an extensive quantity is taken with respect to its own conjugate spatial dimension, orthogonal to each of the other conservation laws. This is in contrast to thermal systems wherein every conservation law is taken with respect to the single, common time dimension. Hence, the analog of the scalar temperature becomes a second-order tensor in granular matter—the stress tensor. Some of the ramifications of this tensorial generalization are discussed in Sec. IV.D.

2. Idealizations of the Ensemble

This analysis focuses upon the thermodynamic limit of 2D, amorphous packings of cohesionless, frictionless, rigid, round grains which have four contacts each. This is a good starting point because 2D packings of cohesionless, round grains that are perfectly rigid [11, 12, 13] and/or frictionless [9, 10, 14, 16, 17, 19, 27] are known to have force distributions with the same qualitative features as the more generalized packings and hence must be subject to the same organizational constraints in the statistics. Therefore they are *sufficient* to elucidate the origin of those constraints in the physics. There are several important arguments that the true, underlying structure in granular physics will be found in the frictionless case whereas frictional degrees of freedom are a perturbation to that underlying structure. The same can be said for non-cohesion, rigidity, and roundness. These arguments will be presented in the discussion in Sec. IV.B.

The use of exactly four contacts per grain, however, is more idealized than has been achieved in typical numerical simulations. Nevertheless, it is acceptable because that is the average coordination number for 2D frictionless packings of round rigid grains which are isostatic

[22, 37], and it will be shown herein that the same qualitative and quantitative features of $P_F(F)$ arise as they do in the more realistic simulations. One ramification of this idealization is that the effects of large polydispersity are probably neglected here, because coordination number is probably highly correlated with grain diameter. (Otherwise, the dispersity of grain diameters is not a consideration in the analysis.) Using four contacts per grain localizes the isostacy to the individual grains, significantly simplifying the analysis. It may not be too hard to extend the transport equation to include delocalized isostacy in which some grains have five contacts and some have three.

Working in the thermodynamic limit allows us to ignore the statistics of the highly-organized boundary layer as contributing insignificantly to the statistics in bulk. It also allows us to simplify the analysis at several points. The thermodynamic limit statistics of amorphous packings are important to develop a rheological theory for typical granulars found in nature and industry.

B. The Phase Space

The locus in phase space of a classical dilute monatomic gas completely defines its state. We wish to define a phase space for granular packings which is similarly complete. A 2D frictionless granular packing of N round, rigid grains is isostatic and therefore contains $2N$ contacts. The phase space therefore requires at least $4N$ phase space axes, half of which define the force on each contact and half of which define the contact angles, $\{F_k, \theta_k \mid k = 1, \dots, 2N\}$. This space is labeled \mathbb{S}_1 . It is possible to define the ordering of the axes so that it is understood which four contacts correspond to the same grain and therefore which grains contact one another. It will not prove necessary to do so explicitly, although this ordering is implicitly assumed to exist. Therefore, the contact force magnitude F_k at contact angle θ_k represents the j^{th} force vector pointing inwardly on the i^{th} grain, \vec{F}_{ij} ($i = 1, \dots, N; j = 1, \dots, 4$), and it also represents the equal and opposite force vector on the contacted grain.

In the thermodynamic limit $N \rightarrow \infty$ this ensemble has Edwards' flat measure, meaning that every metastable state is equally probable,

$$\rho^{(1)} \{F_k, \theta_k \mid k = 1, \dots, 2N\} = \begin{cases} 1 & \text{where the five metastability} \\ & \text{constraints are satisfied} \\ & \text{(listed below)} \\ 0 & \text{elsewhere} \end{cases} \quad (2)$$

Other coordinate systems could be used to represent the same information, and since the Jacobian of transformation between the various coordinate systems is not gen-

erally unity the question should be asked why Edwards' flat measure would apply in this space and not one of the others. Plausibility arguments for the flat measure in \mathbb{S}_1 shall be given in the discussion section.

The five constraints which define the accessible regions of phase space are described below.

1. Newton's second law (N2L) for static equilibrium must be satisfied at each grain individually,

$$\sum_j \vec{F}_{ij} = 0 \quad \forall i. \quad (3)$$

2. No tensile forces are permitted anywhere in the packing,

$$F_k > 0 \quad \forall k, \quad (4)$$

which restricts the DOS to the first "quadrant" of the force axes.

3. (and 4.) The sum of the x component (y component) forces is specified for any one layer of grains normal to the x axis (y axis). For simplicity, this sum will actually be written as a sum over all grains in the packing, whereas it should be taken only over a subset comprising a single layer. However, in the thermodynamic limit of amorphous packings the layers all approach the same number of grains per unit length and so the average Cartesian load per grain or average Cartesian component of force per contact can be calculated equivalently per layer or per packing. The per-packing method is chosen because it does not require us to identify the actual layers in the phase space. Hence,

$$\sum_{i=1}^N w_{xi} = W_x, \quad \sum_{i=1}^N w_{yi} = W_y, \quad (5)$$

where the Cartesian loads on each grain are defined by,

$$w_{xi} = \frac{1}{2} \sum_{j=1}^4 F_{ij} |\cos \theta_{ij}|, \quad w_{yi} = \frac{1}{2} \sum_{j=1}^4 F_{ij} |\sin \theta_{ij}|, \quad (6)$$

and for simplicity these will often be called the "supported loads" or simply the "loads" [41]. The relationship to the stress tensor is $W_x/N = \langle w_{xi} \rangle = \sigma_{xx}/n_x$, where $\langle w_{xi} \rangle$ is the average Cartesian load per grain in the x direction, σ_{xx} is the diagonal element in the stress tensor corresponding to the x direction, and n_x is the number of grains per linear distance, averaged in a cross-sectional layer oriented normal to the x axis.

5. The JPDP for the fabric is specified,

$$\{\theta_k\} \rightarrow P_{4\theta}(\theta_1, \theta_2, \theta_3, \theta_4), \quad (7)$$

meaning that the set of angle coordinates $\{\theta_k\}$ are distributed according to the JPDP $P_{4\theta}(\theta_1, \theta_2, \theta_3, \theta_4)$. Actually, there should be a statement relating the continuum $P_{4\theta}(\theta_1, \theta_2, \theta_3, \theta_4)$ with the discretized distribution of angles at finite N , $\mu_{klmn}(\theta_{1k}, \dots, \theta_{4n})$, but the meaning is nonetheless clear.

In addition to these six constraints, two missing constraints should be noted:

1. The above ensemble does not enforce the shear stresses but relies on the fact that their ensemble average is zero and in the thermodynamic limit the fraction of packings in which the shear deviates from zero by more than some arbitrarily small amount will vanish. The Cartesian axes of the packings are taken to be aligned with the principle stress axes so that the off-diagonal (shear) elements of the stress tensor should indeed be zero.

2. There is one other important omission in the constraints of this ensemble in that the contact angles in a cluster of real grains must form closed loops so that no two grains overlap one another. This intentional omission is of great importance and shall be called the Assumption of Non-recursive Correlation (ANC) because it asserts that only negligible correlative information travels all the way around closed loops of grains in the ensemble average. In other words, the DOS is adequately characterized for the present purposes by the two-point (intra-grain) force correlations and the resulting correlation of loads in neighboring grains. Therefore, the closure of force loops can be ignored when deriving the statistics of single-grain states. There are important arguments supporting the ANC and they will be presented in the discussion section.

C. Phase Space Operations to Quantify the Non-Uniformity

Although Edwards' flat measure is uniform across the regions of accessible phase space, the volume of those regions is not uniformly distributed across the coordinates. The program is to change coordinates in a way that eliminates the constraints from the far right-hand side of Eq. (2), moving a non-uniform set of constraints into a non-uniform DOS. When only the conservation quantities remain in the list of constraints, then the method of the most probable distribution may be used, relying on the method of Lagrange multipliers to conserve those quantities.

1. Newton's Third Law

Newton's third law (N3L) is automatically satisfied in the phase space, since each contact is represented by only one force and one angle axis. However, enforcing N2L will prove simpler if redundant axes are created to account for each contact force twice, one time with each grain that shares the contact, $\{F_{ij}, \theta_{ij} \mid i = 1, \dots, N; j = 1, \dots, 4\}$, where i subscripts the grain and j subscripts the contact on the grain. This space is labeled \mathbb{S}_2 . In this new space it will be necessary to enforce N3L. It is possible to define the ordering of the axes so that it is understood which contacts are redundant to one another and there-

fore which grains are contacting neighbors. It will not be necessary to do so explicitly, although this ordering is implicitly assumed to exist.

In this context the term "grain configuration" refers not only to a grain's contact geometry but also to the set of forces upon those contacts as defined by the locus in phase space. The form of \mathbb{S}_2 itself does not require neighboring grains to satisfy N3L, and so the vast majority of loci include neighboring grain configurations with physically unrealizable forces. This mathematical abstraction enables the analysis.

The DOS in \mathbb{S}_2 is,

$$\rho^{(2)} \{F_{ij}, \theta_{ij} \mid i = 1, \dots, N; j = 1, \dots, 4\} = \begin{cases} 1 & \text{if } \sum_j \vec{F}_{ij} = 0 \forall i, \\ & F_{ij} > 0 \forall (i, j), \\ & \sum_i w_{xi} = W_x, \\ & \sum_i w_{yi} = W_y, \text{ and} \\ & \{\theta_{ij}\} \rightarrow P_{4\theta}(\theta_1, \theta_2, \theta_3, \theta_4), \\ & \vec{F}_{ij} = -\vec{F}_{kl} \text{ (shared contacts)} \\ 0 & \text{elsewhere} \end{cases} \quad (8)$$

The constraints are the same five included in \mathbb{S}_1 , plus a new, sixth constraint: N3L must be satisfied at each contact between grains,

$$\vec{F}_{ij} = -\vec{F}_{kl}, \quad (9)$$

where grains i and k are contacting neighbors and the j^{th} contact on grain i corresponds to the l^{th} contact on grain k .

If we wished to neglect N3L then we could proceed with the remainder of the analysis, obtaining the hypothetical DOS for regions of this space having stable, cohesionless grains, write the state-counting entropy and then maximize it subject to the conservation of total loads and fabric. This would produce the most probable distribution for all possible permutations of N stable grain configurations where the grains are mechanically *independent*. However, it turns out that N3L is not negligible: by considering instead all the possible *combinations* (rather than all possible *permutations*) of N stable, independent grain configurations, we note that some of these combinations can be mechanically connected into a greater number permutations satisfying N3L than can other combinations. Hence, those combinations are the more entropic ones, the ones which represent the greater number of metastable packings in the phase space. Therefore, to find the most entropic combination of stable, independent grain configurations, we will map $\mathbb{S}_2 \rightarrow \mathbb{S}_3$, a space where the axes are the same as in \mathbb{S}_2 except that they are not sequenced to represent a particular permutation of the grains. Whereas a locus in \mathbb{S}_2 represents a single state (a single packing permutation of a set of grain configurations), a locus in \mathbb{S}_3 represents a set of mechanically disconnected grain configurations that may or may not be permutable into some number of stable states. We

shall call the latter an ‘‘assembly space’’ to distinguish it from a phase space that identifies every grain’s location in the packing. The fraction of permutations that satisfy N3L will be quantified in this mapping process.

To verify that a particular permutation of a given combination of stable grains $\{F_{ij}, \theta_{ij}\}$ satisfies N3L, it is necessary to check every contact in the permutation. All permutations of this combination must have the same JPDF of forces and contact angles, $P_{F\theta}(F, \theta) = P_{F\theta}(F, \theta | \{F_{ij}, \theta_{ij}\})$, whatever its form may be. Randomly choosing one contact from the set of these permutations, a contact force F_1 at angle θ_1 has the probability $P_{F\theta}(F_1, \theta_1) dF d\theta$ that it will satisfy N3L with its neighbor. (The two differentials reflect the fact that N3L reduces the solution space by two dimensions per contact, thereby taking out the extra dimensions introduced in $\mathbb{S}_1 \rightarrow \mathbb{S}_2$.) The probability that an entire grain configuration drawn from this set of permutations will satisfy N3L with its four neighbors will be called $\Upsilon^2(F_1, \dots, F_4, \theta_1, \dots, \theta_4) d^4F d^4\theta$, written for compactness as $\Upsilon^2(F_j, \theta_j) d^4F d^4\theta$ [42]. The reason for introducing the square exponent in Υ^2 will become clear momentarily. It may be written as a functional of $P_{F\theta}$,

$$\Upsilon^2(F_j, \theta_j) = \prod_{j=1}^4 P_{F\theta}(F_j, \theta_j). \quad (10)$$

This expression treats the contacts on the neighboring grains as if they are uncorrelated because this is a packing that was drawn randomly from the set of all possible permutations, including the ones which are physically unrealizable. Therefore there are no *a priori* correlations between neighboring grains; such correlations arise *a posteriori* by selecting the subset of packings that satisfy N3L.

Because of this statistical independence, the fraction of packings that satisfy N3L for all of its grains is likewise simply the product over the probabilities that each of the individual grains will satisfy N3L with its own local neighbors. (The ANC appears implicitly in this statement.) However, the product of Υ^2 over every grain accounts for every contact in the packing twice, once with each grain sharing the contact. For the cases where N3L is in fact satisfied, the double accounting of contacts will appear as pairs of $P_{F\theta}$ factors having identical arguments. Hence, the probability that the entire packing will satisfy N3L is the square root of that product. This is why the the square exponent was written in Eq. (10). The fraction of permutations that satisfy N3L shall be called $\Phi_{\text{N3L}}(F_{11}, \dots, F_{N4}, \theta_{11}, \dots, \theta_{N4})$, written as $\Phi_{\text{N3L}}\{F_{ij}, \theta_{ij}\}$ for compactness.

$$\Phi_{\text{N3L}}\{F_{ij}, \theta_{ij}\} = \prod_{i=1}^N \Upsilon(F_{ij}, \theta_{ij}) d^{2N}F d^{2N}\theta. \quad (11)$$

This calculation does not handle the boundaries of the packing (unless they are periodic), but we are concerned

with the statistics in the bulk in the thermodynamic limit where the boundaries are pushed out toward infinity.

Now we may map the DOS from the phase space to the assembly space, $\mathbb{S}_2 \rightarrow \mathbb{S}_3$. Showing the functional dependence upon $P_{F\theta}$ explicitly, the DOS in \mathbb{S}_3 is,

$$\begin{aligned} \tilde{\rho}^{(3)}\{F_{ij}, \theta_{ij}\} &= \\ &= \begin{cases} N! \prod_i \Upsilon(F_{ij}, \theta_{ij}) \left[P_{F\theta}(F_{ij}, \theta_{ij} | \{F_{ij}, \theta_{ij}\}) \right] \\ \quad \times d^{2N}F d^{2N}\theta \\ \\ \text{if } \begin{cases} \sum_j \vec{F}_{ij} = 0 \forall i, \\ F_{ij} > 0 \forall (i, j), \\ \sum_i w_{xi} = W_x, \\ \sum_i w_{yi} = W_y, \text{ and} \\ \{\theta_{ij}\} \rightarrow P_{4\theta}(\theta_1, \theta_2, \theta_3, \theta_4) \end{cases} \\ \\ 0 \text{ elsewhere.} \end{cases} \end{aligned} \quad (12)$$

The tilde on $\tilde{\rho}$ indicates that this density is in an assembly space.

2. Newton’s Second Law

To quantify the effects of N2L, note that Eq. (6) is a many-to-one mapping from \mathbb{S}_2 to a space $\{w_{xi}, w_{yi}, \theta_{ij} | i = 1, \dots, N; j = 1, \dots, 4\}$. Thus, the mapping reduces the dimensionality of the space by two per grain, just as N2L reduces the dimensionality of the solution space by two per grain. However, the reverse mapping is one-to-one because the localized isostacy of the grains determines the four contact forces when the supported loads and four contact angles are specified. Thus, of all the points in \mathbb{S}_2 that map to the same point in $\{w_{xi}, w_{yi}, \theta_{ij}\}$, at most only one represents a stable packing and is occupied, the one which is specified in the return direction by

$$\vec{F} = A^{-1} \vec{W}, \quad (13)$$

where

$$\begin{aligned} \vec{F} &= \begin{Bmatrix} F_{11} \\ F_{12} \\ \vdots \\ F_{N4} \end{Bmatrix}, \\ \vec{W} &= \begin{Bmatrix} w_{x1} \\ w_{x1} \\ w_{y1} \\ w_{y1} \\ w_{x2} \\ w_{x2} \\ \vdots \\ w_{yN} \\ w_{yN} \end{Bmatrix}, \end{aligned} \quad (14)$$

and where A is block diagonal with 4×4 blocks $\mathcal{A}^{(i)} = \mathcal{A}^{(i)}(\theta_{i1}, \dots, \theta_{i4})$ that are superscripted by the grain index ($i = 1, \dots, N$). The elements of $\mathcal{A}^{(i)}$ are $a_{kj}^{(i)}$ in the k^{th} row and j^{th} column,

$$\begin{aligned} a_{1j}^{(i)} &= R_{ij} \cos \theta_{i1}, \\ a_{2j}^{(i)} &= -L_{ij} \cos \theta_{i2}, \\ a_{3j}^{(i)} &= T_{ij} \sin \theta_{i3}, \\ a_{4j}^{(i)} &= -B_{ij} \sin \theta_{i4}. \end{aligned} \quad (15)$$

The operator R_{ij} multiplies the expression by 1 if $-\pi/2 \leq \theta_{ij} < \pi/2$ meaning the j^{th} contact is on the right half of the grain, else it multiplies it by 0. Likewise L_{ij} , T_{ij} and B_{ij} test for contacts on the left, top and bottom side of the grain, respectively. This matrix is nonsingular except for some precise alignments of contacts on a grain which we can ignore, so each point in the new space corresponds to a single stable point in \mathbb{S}_2 .

While it is straightforward to write down the expression for generalized fabrics using these R , L , T , and B operators, the expressions often become cumbersome. For the sake of simplicity in the expressions, we shall introduce the idea of ‘‘quartered’’ fabric in which $P_{4\theta}(\theta_1, \dots, \theta_4)$ is zero everywhere except where the j^{th} contact is on the j^{th} quadrant of every grain in the packing. The orientation of the j^{th} quadrant is defined the usual way as $(j-1)\pi/2 < \theta < j\pi/2$ in \mathbb{S}_2 . As in the case of non-quartered fabric, $J_{4\theta}$ enforces steric exclusion. For the specific case of ‘‘quartered isotropy,’’ collapsing the quartered fabric by Eq. (1) produces $P_\theta(\theta) = 1/2\pi$. This mimics true isotropy but the anisotropic quartering is nevertheless apparent in the JPFD $P_{4\theta}(\theta_1, \dots, \theta_4)$. To achieve quartered isotropy with steric exclusion in a Monte Carlo process it is necessary to weight the distribution of attempted angles to emphasize the regions close to the edges of each quadrant. Otherwise, steric exclusion would cause notches to appear in $P_\theta(\theta)$ near the boundary of each quadrant. The use of quartered fabric in this analysis is only for illustrative simplicity, so that the meaning of the expressions may be intuitively grasped. It is always possible to write and numerically solve the expressions in a form that represents more general fabric.

For the illustrative case of quartered fabric,

$$\mathcal{A}^{(i)} = \begin{pmatrix} \cos \theta_{i1} & 0 & 0 & \cos \theta_{i4} \\ 0 & \cos \theta_{i2} & \cos \theta_{i3} & 0 \\ \sin \theta_{i1} & \sin \theta_{i2} & 0 & 0 \\ 0 & 0 & \sin \theta_{i3} & \sin \theta_{i4} \end{pmatrix}. \quad (16)$$

We will use the mapping of Eq. (6) to go from $\mathbb{S}_3 \rightarrow \mathbb{S}_4$, which will have coordinates $\{w_{xi}, w_{yi}, \theta_{ij}\}$ and is another assembly space, representing combinations of mechanically-independent grain configurations. By changing to the new \mathbb{S}_4 coordinates we have automatically enforced N2L, eliminating all the loci in \mathbb{S}_3 where N2L is not satisfied. The Jacobian of transformation for

$\mathbb{S}_3 \rightarrow \mathbb{S}_4$ is $J_{34} = \prod_i |\det \mathcal{A}^{(i)}|^{-1} (dF)^{-2N}$, so the DOS in this space is,

$$\begin{aligned} \tilde{\rho}^{(4)}\{w_{xi}, w_{yi}, \theta_{ij}\} &= \\ &= \begin{cases} N! d^{2N}\theta \prod_i |\det \mathcal{A}^{(i)}|^{-1} \\ \quad \times \Upsilon(F_{ij}, \theta_{ij}) \left[P_{F\theta}(F, \theta \mid \{F_{ij}, \theta_{ij}\}) \right], \\ \quad \text{if } F_{ij} > 0 \forall (i, j), \\ \quad \sum_i w_{xi} = W_x, \\ \quad \sum_i w_{yi} = W_y, \text{ and} \\ \quad \{\theta_{ij}\} \rightarrow P_{4\theta}(\theta_1, \theta_2, \theta_3, \theta_4) \\ 0 \text{ elsewhere} \end{cases} \end{aligned} \quad (17)$$

where $F_{ij} = F_{ij}(w_{xi}, w_{yi}, \theta_{i1}, \dots, \theta_{i4})$. Or, using delta functions to produce the Jacobian, it may be written,

$$\begin{aligned} \tilde{\rho}^{(4)}\{w_{xi}, w_{yi}, \theta_{ij}\} &= \\ &= \begin{cases} N! d^{2N}\theta \times \\ \quad \prod_i \Upsilon_w(w_{xi}, w_{yi}, \theta_{ij}) \left[P_{F\theta}(F, \theta \mid \{w_{xi}, w_{yi}, \theta_{ij}\}) \right], \\ \quad \text{if } F_{ij} > 0 \forall (i, j), \\ \quad \sum_i w_{xi} = W_x, \\ \quad \sum_i w_{yi} = W_y, \text{ and} \\ \quad \{\theta_{ij}\} \rightarrow P_{4\theta}(\theta_1, \theta_2, \theta_3, \theta_4) \\ 0 \text{ elsewhere} \end{cases} \end{aligned} \quad (18)$$

where, in the special case of quartered isotropy,

$$\begin{aligned} \Upsilon_w^2(w_x, w_y, \theta_j) &= \iiint \int_o^\infty d^4F \prod_{j=1}^4 P_{F\theta}(F_j, \theta_j) \\ &\quad \times \delta(w_x - F_1 \cos \theta_1 - F_4 \cos \theta_4) \\ &\quad \times \delta(w_x + F_2 \cos \theta_2 + F_3 \cos \theta_3) \\ &\quad \times \delta(w_y - F_1 \sin \theta_1 - F_2 \sin \theta_2) \\ &\quad \times \delta(w_y + F_3 \sin \theta_3 + F_4 \sin \theta_4). \end{aligned} \quad (19)$$

3. Cohesionless Grains

While $\mathbb{S}_3 \rightarrow \mathbb{S}_4$ eliminated all unstable grain configurations, not every point in \mathbb{S}_4 maps to the first quadrant of the force axes in \mathbb{S}_3 because some combinations of $(w_x, w_y, \theta_1, \dots, \theta_4)$ require one or two tensile contacts for stability. These, too, are unstable grain configurations for cohesionless packings. If we enforce the condition that $P_{F\theta}(F, \theta) = 0$ for $F < 0$, then the form of Υ in Eq. (19) will automatically enforce the cohesionless constraint. However, it will prove convenient to express the

non-tensile constraint explicitly,

$$\begin{aligned} \tilde{\rho}^{(4)}\{w_{xi}, w_{yi}, \theta_{ij}\} &= \\ &= \begin{cases} N! d^{2N} \theta \prod_i \Psi(w_{xi}, w_{yi}, \theta_{ij}) \\ \quad \times \Upsilon_w(w_{xi}, w_{yi}, \theta_{ij}) [P_{F\theta}(F, \theta | \{F_{ij}, \theta_{ij}\})], \\ \quad \text{if } \begin{cases} \sum_i w_{xi} = W_x, \\ \sum_i w_{yi} = W_y, \text{ and} \\ \{\theta_{ij}\} \rightarrow P_{4\theta}(\theta_1, \theta_2, \theta_3, \theta_4) \end{cases} \\ 0 \text{ elsewhere} \end{cases} \end{aligned} \quad (20)$$

where $\Psi(w_{xi}, w_{yi}) = \prod_{j=1}^4 \Theta(F_{ij})$ with Θ being the Helmholtz (unit step) function, whose arguments $F_{ij} = F_{ij}(w_{xi}, w_{yi}, \theta_{ij})$.

D. State-Counting Entropy and Its Maximum

Randomly drawing packings from the regions of \mathbb{S}_4 that have the correct fabric and specified $P_{F\theta}(F, \theta)$ and specified $P_{2w4\theta}(w_x, w_y, \theta_1, \dots, \theta_4)$, the fraction of packings in which all grains will satisfy N2L without cohesion and satisfy N3L with its neighbors is therefore,

$$\begin{aligned} \Phi\{w_{xi}, w_{yi}, \theta_{ij}\} [P_{F\theta}] &= \\ &= \prod_i \Upsilon_w(w_{xi}, w_{yi}, \theta_{ij}) [P_{F\theta}] \cdot \Psi(w_{xi}, w_{yi}, \theta_{ij}) d^{2N} \theta \\ &= \prod_i \cdots \prod_n \left[\Upsilon_w(w_{xi}, w_{yj}, \theta_{1k}, \dots, \theta_{4n}) [P_{F\theta}] \right. \\ &\quad \left. \times \Psi(w_{xi}, w_{yj}, \theta_{1k}, \dots, \theta_{4n}) \right]^{\nu_{ijklmn}} d^{2N} \theta \end{aligned} \quad (21)$$

where $\nu_{ijklmn}(w_{xi}, w_{yj}, \theta_{1k}, \dots, \theta_{4n})$ is the discretized version of the distribution $P_{2w4\theta}(w_x, w_y, \theta_1, \dots, \theta_4)$, normalized such that $\sum_i \cdots \sum_n \nu_{ijklmn} = N$. It was obtained by discretizing the $(w_x, w_y, \theta_1, \dots, \theta_4)$ space into bins of volume $(\Delta w_x \cdot \Delta w_y \cdot \Delta \theta_1 \cdots \Delta \theta_4) = (\Delta w)^2 (\Delta \theta)^4$. Note that in Eq. (21), the sum in the first line is over the grains whereas the sums in the second line are over the discretized intervals of each of the variables $w_x, w_y, \theta_1, \dots, \theta_4$. For compactness we will write,

$$\Phi\{w_{xi}, w_{yi}, \theta_{ij}\} [P_{F\theta}] = \prod_i \cdots \prod_n \left[\Upsilon_{i\dots n} \cdot \Psi_{i\dots n} \right]^{\nu_{i\dots n}} d^{2N} \theta. \quad (22)$$

To find the most probable $P_{2w4\theta}(w_x, w_y, \theta_1, \dots, \theta_4)$ that results from the non-uniform DOS of Eq. (18), we likewise discretize \mathbb{S}_4 into cells of volume $(\delta w_x \cdot \delta w_y \cdot \delta \theta_1 \cdots \delta \theta_4)^N$ where $(\delta w)^2 (\delta \theta)^4 = (\Delta w)^2 (\Delta \theta)^4 / S$, where S is a large integer and $S \gg \nu_{i\dots n} \forall (i, \dots, n)$. The number of cells in \mathbb{S}_4 which map to a particular set $\{\nu_{i\dots n}\}$

can be estimated by explicit counting,

$$\begin{aligned} \omega\{\nu_{i\dots n}\} &= \prod_i \cdots \prod_n \left[\frac{(S-1 + \nu_{i\dots n})!}{(S-1)! (\nu_{i\dots n})!} \right] \\ &\quad \times \left(\sum_i \cdots \sum_n \nu_{i\dots n} \right)! \end{aligned} \quad (23)$$

and in the limit as $S \rightarrow \infty$ the estimate becomes exact. However, because \mathbb{S}_4 is an assembly space, the axes can be relabeled $N!$ different ways to represent the same combination of grains. Removing this physically meaningless repetition, we omit the factorial of the sums in the second line of Eq. (23),

$$\tilde{\omega}\{\nu_{i\dots n}\} = \prod_i \cdots \prod_n \left[\frac{(S-1 + \nu_{i\dots n})!}{(S-1)! (\nu_{i\dots n})!} \right], \quad (24)$$

where the tilde on $\tilde{\omega}$ indicates that this is the ‘‘correct Boltzmann counting’’ for an assembly space, in which the grains are indistinguishable.

The number of states Ω in the ensemble mapping to the distribution $\{\nu_{i\dots n}\}$ is therefore $\tilde{\omega}\{\nu_{i\dots n}\}$ times the DOS in those cells of \mathbb{S}_4 ,

$$\begin{aligned} \Omega\{\nu_{i\dots n}\} &= \prod_i \cdots \prod_n \left[\frac{(S-1 + \nu_{i\dots n})!}{(S-1)! (\nu_{i\dots n})!} \right] \\ &\quad \times N! [\Upsilon_{i\dots n} \Psi_{i\dots n}]^{\nu_{i\dots n}} d^{2N} \theta \end{aligned} \quad (25)$$

where we have used the notation of Eq. (22) to express the DOS. Taking the logarithm, it may be maximized with respect to $\nu_{p\dots u}$. If we discretize the JPDF of fabric $P_{4\theta}(\theta_1, \dots, \theta_4) \rightarrow \mu_{klmn}(\theta_k, \dots, \theta_n)$ such that $\sum_k \cdots \sum_n \mu_{klmn} = N$, then each value of $\mu_{klmn} \forall k, l, m, n$ is a conserved quantity according to the definition of the ensemble in which fabric is specified. The conservation of W_x, W_y and μ_{klmn} are enforced via Lagrange multipliers ξ_x, ξ_y and γ_{klmn} respectively.

$$\begin{aligned} \frac{\partial}{\partial \nu_{p\dots u}} \left[\ln \Omega\{\nu_{i\dots n}\} - \xi_x \left(\sum_i \cdots \sum_n \nu_{i\dots n} w_{xi} \right) \right. \\ \left. - \xi_y \left(\sum_i \cdots \sum_n \nu_{i\dots n} w_{yj} \right) \right. \\ \left. - \sum_k \cdots \sum_n \gamma_{k\dots n} \left(\sum_i \sum_j \nu_{i\dots n} \right) \right] = 0 \end{aligned} \quad (26)$$

The calculus is performed using Stirling’s approximation and an expansion of the logarithm in a Taylor series of $\nu_{i\dots n}$ where necessary. Taking the limit for $S \rightarrow \infty$ while conserving N and then taking the continuum limit obtains

$$\begin{aligned} P_{2w4\theta}(w_x, w_y, \theta_j) &= \Upsilon_w(w_x, w_y, \theta_j) \Psi(w_x, w_y, \theta_j) \\ &\quad \times G(\theta_j) e^{-\xi_x w_x - \xi_y w_y} \end{aligned} \quad (27)$$

where $G(\theta_j) = G(\theta_1, \dots, \theta_4)$ derives from $\exp(-\gamma_{p\dots u})$ in the continuum limit.

Note that ξ_x and ξ_y should not be confused with the decay constants of the exponential tails in the empirical PDFs. Most (if not all) of the exponential behavior in Eq. (27) is contained in the form of Υ_w because it is a functional of $P_{F\theta}(F, \theta)$. It will be shown in a numerical solution of the isotropic case using an approximation method (later in this paper) that the value of $\xi_x = \xi_y$ is approximately zero. This should not be the case in general, however because these two parameters provide the only information about stress anisotropy in the equation.

E. The Fabric Partition Factor

The Fabric Partition Factor G , along with Υ and Ψ , determines the partition of fabric between the (w_x, w_y) “modes”. Integrating Eq. (27) over w_x and w_y

$$\begin{aligned} P_{4\theta}(\theta_j) &= G(\theta_j) \iint_0^\infty d^2w \Upsilon_w \Psi e^{-\xi_x w_x - \xi_y w_y} \\ &= G(\theta_j) H(\theta_j). \end{aligned} \quad (28)$$

Using the definitions of Ψ and Υ_w for the case of quartered fabric,

$$\begin{aligned} H(\theta_1, \dots, \theta_4) &= \iint_0^\infty d^2w e^{-\xi_x w_x - \xi_y w_y} \\ &\times \left\{ \iiint_0^\infty \int_0^\infty d^4 \prod_{j=1}^4 P_{F\theta}(F_j, \theta_j) \right. \\ &\times \delta(w_x - F_1 \cos \theta_1 - F_4 \cos \theta_4) \\ &\times \delta(w_x + F_2 \cos \theta_2 + F_3 \cos \theta_3) \\ &\times \delta(w_y - F_1 \sin \theta_1 - F_2 \sin \theta_2) \\ &\times \left. \delta(w_y + F_3 \sin \theta_3 + F_4 \sin \theta_4) \right\}^{\frac{1}{2}} \\ &\times \left\{ \prod_{j=1}^4 \Theta[F_j(w_x, w_y, \theta_1, \dots, \theta_4)] \right\} \end{aligned} \quad (29)$$

For the case of quartered fabric, Eq. (19), some manipulation obtains

$$\begin{aligned} H(\theta_1, \dots, \theta_4) &= \left[\prod_{j=1}^4 \int_0^\infty dF_j P_{F\theta}(F_j, \theta_j) \right. \\ &\times \left. e^{-(\xi_x |\cos \theta_j| + \xi_y |\sin \theta_j|) F_j} \right]^{\frac{1}{2}}, \end{aligned} \quad (30)$$

where each term of the product is a Laplace transform $\mathcal{L}[P_{F\theta}(F, \theta); u] = \tilde{P}_{F\theta}(u, \theta)$ with the transform variable $u_j = u_j(\theta_j) = \xi_x |\cos \theta_j| + \xi_y |\sin \theta_j|$. Therefore, the Fabric Partition Factor is,

$$G(\theta_1, \dots, \theta_4) = P_{4\theta}(\theta_1, \dots, \theta_4) \prod_{j=1}^4 \tilde{P}_{F\theta}^{-\frac{1}{2}}(u(\theta_j), \theta_j). \quad (31)$$

Assuming the standard result of statistical mechanics, one form of $P_{F\theta}$ will be found in the overwhelming majority of the occupied phase space, and so in the thermodynamic limit we may treat fabric as if it is partitioned by G with a fixed form of $\tilde{P}_{F\theta}$ in all of phase space. This factor is not a function of w_x or w_y . However, the partition is not an equipartition because of the influence of Υ and Ψ . The former is variable over the range of angle configurations within each mode, and the second is a truncating factor which limits the range of angle configurations within each mode.

F. The Recursive “Transport” Equation

The JPDF $P_{2w4\theta}$ can be collapsed,

$$\begin{aligned} P_{F\theta}(F, \theta) &= \frac{1}{4} \sum_{j=1}^4 \iint_0^\infty d^2w \iiint_0^{2\pi} d^4\theta \delta(\theta - \theta_j) \\ &\times \delta[f - f_j(w_x, w_y, \theta_1, \dots, \theta_4)] \\ &\times P_{2w4\theta}(w_x, w_y, \theta_1, \dots, \theta_4). \end{aligned} \quad (32)$$

Inserting Eq. (27) into Eq. (32) results in a recursion of $P_{F\theta}$,

$$\begin{aligned} P_{F\theta}(F, \theta) &= \frac{1}{4} \sum_{j=1}^4 \iint_0^\infty d^2w e^{-\xi_x w_x - \xi_y w_y} \iiint_0^{2\pi} d^4\theta \delta(\theta - \theta_j) \delta[f - f_j(w_x, w_y, \theta_1, \dots, \theta_4)] \\ &\times G(\theta_1, \dots, \theta_4) \prod_{j=1}^4 \Theta[F_{ij}(w_x, w_y, \theta_1, \dots, \theta_4)] \iiint_0^\infty d^4 F' \prod_{k=1}^4 [P_{F\theta}(F'_k, \theta_k)]^{\frac{1}{2}} \\ &\times \delta[w_x - w_x^{\text{right}}(F'_1, \theta_1, \dots, F'_4, \theta_4)] \delta[w_x - w_x^{\text{left}}(\cdot)] \delta[w_y - w_y^{\text{top}}(\cdot)] \delta[w_y - w_y^{\text{bottom}}(\cdot)] \end{aligned} \quad (33)$$

This can be simplified by taking advantage of symmetries in the ensemble. For example, in the case in which fab-

ric is not quartered so that every contact ($j = 1, \dots, 4$)

is statistically similar, then the summation may be removed.

The dependency of Υ upon the form of $P_{F\theta}(F, \theta) = P_{F\theta}(F, \theta \mid \{w_{xi}, w_{yi}, \theta_{ij}\})$ reveals that the DOS in a granular ensemble is self-organized (accomplished by the packing in its dynamic state as it sought a stable locus in phase space) and cannot be given a simplistic *a priori* characterization in a way that is analogous to the *a priori* uniform characterization of a thermal DOS. The form of $P_{F\theta}(F, \theta)$ derives from the DOS non-uniformity and *vice versa*. Hence, without additional knowledge of the DOS, only the recursion equation method can be used to solve $P_{F\theta}(F, \theta)$. In principle, this recursion is the unique solution. However, it should be remembered that this assumes that correlative information is non-recursive in the ensemble average and that Edwards' flat measure is correct.

G. The Mean Structure Approximation

The recursion equation can be solved using Monte Carlo integration. Efforts are underway to obtain the numerical solution, which shall be presented in a future publication. For the present an approximation will be introduced, simplifying the recursion equation while yet providing sufficient accuracy to demonstrate the principle organizational features of the ensemble. The approximation has value in its own right because it will isolate and identify those organizational features.

The approximation is obtained by projecting the DOS in $\mathbb{S}_4 \rightarrow \mathbb{S}_5$, where the latter is the subspace $\{w_{xi}, w_{yi}\}$. This projection is performed by integrating the DOS across all the angle axes. For a given pair of values (w_{x1}, w_{y1}) , the evaluation of $\Upsilon_w(w_{x1}, w_{y1}, \theta_{ij}) \neq \Upsilon_w(w_{x1}, w_{y1}, \theta_{kj})$ for $\{\theta_j\}_i \neq \{\theta_j\}_k$ in general. That is, certain contact angle configurations $\{\theta_j\}$ will yield a greater probability that the grain will be consistent with their neighbors than will other contact angle configurations. Therefore, information is lost in the projection into the \mathbb{S}_5 subspace. Nevertheless, this loss of information may not be so great that it blurs the principle organization of the DOS. Arguments can be advanced to show that, over the distribution of all contact angle configurations where the grain is stable,

$$\Upsilon_w(w_{x1}, w_{y1}, \theta_{ij}) \approx \bar{\Upsilon}(w_{x1}, w_{y1}) \quad (34)$$

for *most* stable grain configurations. Whereas Ψ is a truncating factor in the DOS, defining the region where individual grains are stable, Υ is a scaling factor in the DOS, indicating how often particular grain configurations will occur in the ensemble based upon the probability that they can satisfy N3L with their neighbors. Eq. (34) claims that this scaling is strongly dependent upon the values of w_x and w_y ; but when varying the contact angles it does not vary too much over the majority of that configuration space. This allows the $\mathbb{S}_4 \rightarrow \mathbb{S}_5$ projection to be simplified.

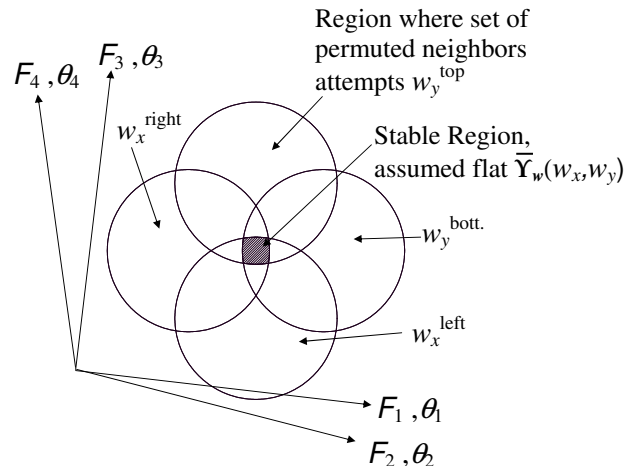


FIG. 2: Iconic diagram of 8-dimensional space to illustrate the Mean Structure Approximation (MSA). The MSA assumes that the probability for a grain to satisfy Newton's third law with its neighbors does not vary over any of the configurations of the grain having fixed Cartesian loads. In fact, the exact probability does not vary too widely for the vast majority of those grain configurations. Therefore, the MSA should produce a distribution of grain configurations that is a good representation of the exact ensemble. The individual circles represent the region where random grain configurations, taken to be neighbors for the grain in question, would attempt to apply a particular load on each hemisphere of that grain. The intersection is the stable region where the MSA applies.

The approximation shall be called the “Mean Structure Approximation,” or MSA, and it is illustrated in Fig. 2. It is important to distinguish this from the Mean Field Approximation (or MFA), which is useful for thermal systems but not acceptable for granular packings. The reason that the MSA may be adequate where the MFA fails is because it preserves the exact intra-grain correlation of contact forces by N2L and also the approximate inter-grain correlations of (w_{xi}, w_{yi}) by N3L, both of which are lost in the MFA. The validity of the MSA shall be evaluated in the discussion section.

The most probable $P_{2w}(w_x, w_y)$ to occur in the \mathbb{S}_5 subspace can be obtained directly by integrating Eq. (27) over all angles,

$$P_{2w}(w_x, w_y) = e^{-\xi_x w_x - \xi_y w_y} \iiint \int_0^{2\pi} d^4\theta G(\theta_j) \times \Psi(w_x, w_y, \theta_j) \Upsilon_w(w_x, w_y, \theta_j) \quad (35)$$

We wish to simplify this in the MSA. Re-writing Eq. (19),

$$\begin{aligned} \Upsilon_w(w_x, w_y, \theta_j) = & \left\{ \iiint\limits_0^\infty \int\limits_0^\infty \int\limits_0^\infty \int\limits_0^\infty d^4 w \iiint\limits_0^\infty \int\limits_0^\infty \int\limits_0^\infty \int\limits_0^\infty d^4 F \right. \\ & \times \delta(w_x^{\text{Right}} - F_1 \cos \theta_1 - F_4 \cos \theta_4) \\ & \times \delta(w_x^{\text{Left}} + F_2 \cos \theta_2 + F_3 \cos \theta_3) \\ & \times \delta(w_y^{\text{Top}} - F_1 \sin \theta_1 - F_2 \sin \theta_2) \\ & \times \delta(w_y^{\text{Bottom}} + F_3 \cos \theta_3 + F_4 \cos \theta_4) \\ & \times \delta(w_x - w_x^{\text{right}}) \delta(w_y - w_y^{\text{top}}) \\ & \times \delta(w_x - w_x^{\text{left}}) \delta(w_y - w_y^{\text{bottom}}) \\ & \left. \times \prod_{j=1}^4 P_{F\theta}(F_j, \theta_j) \right\}^{1/2}, \end{aligned} \quad (36)$$

evaluating the four inner integrals, and commuting the square root with the delta function integrals,

$$\begin{aligned} \Upsilon_w(w_x, w_y, \theta_j) = & \iiint\limits_0^\infty \int\limits_0^\infty \int\limits_0^\infty d^4 w [P_{4w4\theta}^*(w_\xi^\alpha, \theta_j)]^{\frac{1}{2}} \\ & \times \delta(w_x - w_x^{\text{right}}) \delta(w_y - w_y^{\text{top}}) \\ & \times \delta(w_x - w_x^{\text{left}}) \delta(w_y - w_y^{\text{bottom}}) \end{aligned} \quad (37)$$

where,

$$\begin{aligned} P_{4w4\theta}^*(w_\xi^\alpha, \theta_j) = & P_{4w4\theta}^*(w_x^{\text{right}}, \dots, w_y^{\text{bottom}}, \theta_j) \\ = & \iiint\limits_0^\infty \int\limits_0^\infty \int\limits_0^\infty d^4 F \prod_{j=1}^4 P_{F\theta}(F_j, \theta_j) \\ & \times \delta(w_x^{\text{right}} - F_1 \cos \theta_1 - F_4 \cos \theta_4) \\ & \times \delta(w_x^{\text{left}} + F_2 \cos \theta_2 + F_3 \cos \theta_3) \\ & \times \delta(w_y^{\text{top}} - F_1 \sin \theta_1 - F_2 \sin \theta_2) \\ & \times \delta(w_y^{\text{bottom}} + F_3 \sin \theta_3 + F_4 \sin \theta_4). \end{aligned} \quad (38)$$

This can be interpreted as the JPDF of *attempted* loads and contact angles that the set of all possible packing permutations (with the specified $P_{F\theta}$) *attempts* to place on any one grain. The star indicates that this is only a conceptual distribution, not found in stable packings. It can be viewed as a mean-field calculation, where the incoming forces have been drawn randomly from the entire set of grains in the packing permutations. Its domain is therefore not restricted to the set of forces that would make a grain stable. Because of this, the pair $(w_x^{\text{right}}, w_y^{\text{top}})$ should not be too strongly correlated to $(w_x^{\text{left}}, w_x^{\text{bottom}})$ after integrating out the angular dependence,

$$\begin{aligned} P_{4w}^*(w_x^{\text{right}}, w_y^{\text{top}}, w_x^{\text{left}}, w_y^{\text{bottom}}) \approx & \\ P_{2w}^*(w_x^{\text{right}}, w_y^{\text{top}}) P_{2w}^*(w_x^{\text{left}}, w_y^{\text{bottom}}). \end{aligned} \quad (39)$$

All the angular content of Υ_w is in $P_{4w4\theta}^*(w_\xi^\alpha, \theta_j)$, so we make the mean structure approximation,

$$P_{4w4\theta}^*(w_\xi^\alpha, \theta_j) \approx P_{4w}^*(w_\xi^\alpha) / 16\pi^4 \quad (40)$$

for *most* stable grain configurations, so that by Eq. (37),

$$\Upsilon(w_x, w_y, \theta_j) \approx [P_{4w}^*(w_x, w_x, w_y, w_y)]^{\frac{1}{2}} / 4\pi^2 \quad (41)$$

for most $\{w_x, w_y, \theta_j\}$. Using Eqs. (34), (39), and (41) we define

$$\bar{\Upsilon}(w_x, w_y) = P_{2w}^*(w_x, w_y) / 4\pi^2. \quad (42)$$

$P_{2w}^*(w_x, w_y)$ may be viewed as a mean-field calculation of *attempted* loads (for packing permutations having the specified $P_{F\theta}$), which the half-space of the ensemble attempts to place on the corresponding hemisphere of a grain (for each of the two Cartesian loads), and where the mean field includes the unstable regions of the phase space. However, it must be emphasized that this is not a mean-field calculation of loads actually placed on the grains, but rather it is the approximate scale measuring how often particular modes will satisfy N3L and therefore occur in the ensemble. The validity of the approximation depends on the relative weakness of Υ 's dependency on the contact angles for most stable grain configurations.

Using the MSA in Eq. (35),

$$\begin{aligned} P_{2w}(w_x, w_y) = & e^{-\xi_x w_x - \xi_y w_y} \bar{\Upsilon}(w_x, w_y) \\ & \times \iiint\limits_0^{2\pi} \int\limits_0^{2\pi} \int\limits_0^{2\pi} d^4 \theta G(\theta_j) \Psi(w_x, w_y, \theta_j) \end{aligned} \quad (43)$$

Defining,

$$\begin{aligned} \bar{\Psi}(w_x, w_y) = & \iiint\limits_0^{2\pi} \int\limits_0^{2\pi} \int\limits_0^{2\pi} d^4 \theta G(\theta_j) \\ & \times \prod_{k=1}^4 \Theta[F_k(w_x, w_y, \theta_1, \dots, \theta_4)]. \end{aligned} \quad (44)$$

we may write,

$$P_{2w}(w_x, w_y) = e^{-\xi_x w_x - \xi_y w_y} \bar{\Upsilon}(w_x, w_y) \bar{\Psi}(w_x, w_y) \quad (45)$$

Writing the DOS in the $\{w_x, w_y\}$ subspace, another assembly space labeled \mathbb{S}_5 ,

$$\begin{aligned} \tilde{\rho}^{(5)}\{w_{xi}, w_{yi}\} = & \\ = & \begin{cases} N! \prod_i \bar{\Upsilon}(w_{xi}, w_{yi}) \bar{\Psi}(w_{xi}, w_{yi}), & \text{if } \sum_i w_{xi} = W_x, \\ & \sum_i w_{yi} = W_y, \text{ and} \\ 0 \text{ elsewhere} \end{cases} \end{aligned} \quad (46)$$

We identify $\overline{\Psi}(w_x, w_y)$ as the ‘‘Grain Factor’’ and $\overline{\Upsilon}(w_x, w_y)$ as the ‘‘Structure Factor.’’ These are the primary features of non-uniformity in the DOS. Whereas $\overline{\Psi}$ derives from the configuration space of *individual* grains (cohesionless N2L), $\overline{\Upsilon}$ derives from the configuration space of grains connecting together to form a packing structure (N3L). These two factors were so-named because their separability (in the MSA) and their roles may be considered somewhat analogous to the separability and roles of the atomic form factor and structure factor of x-ray crystallography.

The meaning of the $\overline{\Psi}$ can be illustrated easily through a change a variables. We notice that for rigid, cohesionless grains there is no inherent force scale and hence stability must be independent of the overall scale of the forces. Thus it is convenient to change variables,

$$s_i = \frac{w_{xi} - w_{yi}}{w_{xi} + w_{yi}}, \quad t_i = w_{xi} + w_{yi}. \quad (47)$$

The stability of the i^{th} grain is therefore a function of s_i and the four contact angles, $\{\theta_j\}_i$, only. With the Jacobian $J = t$, Eq. (35) can also be written,

$$P_{st}(s, t) = \overline{\Upsilon}_{st}(s, t) \overline{\Psi}_s(s) e^{-(\xi_x + \xi_y)t/2 - (\xi_x - \xi_y)st/2} \quad (48)$$

where the notation has been introduced,

$$\begin{aligned} \overline{\Upsilon}_{st}(s, t) &= t \overline{\Upsilon}[(1+s)t/2, (1-s)t/2] \\ &= (w_x + w_y) \overline{\Upsilon}(w_x, w_y), \end{aligned} \quad (49)$$

and,

$$\begin{aligned} \overline{\Psi}_s(s) &= \overline{\Psi}[(1+s)t/2, (1-s)t/2] \\ &= \overline{\Psi}(w_x, w_y). \end{aligned} \quad (50)$$

Note that Θ in Eq. (44) is insensitive to the scale of F_k and cares only whether it is positive or negative, and hence the t does not appear as an argument of $\overline{\Psi}_s(s)$.

In these coordinates Eq. (44) may be solved very efficiently by Monte Carlo integration. This has been performed for the case of quartered isotropy. In the MSA, $\overline{\Upsilon}$ does not affect the fabric partition, and hence it is easy to find the fabric partition factor. The product of the weighting for the quartering bias with the weighting for the fabric partition was obtained empirically by adjusting as required in a Fourier decomposition to achieve approximate isotropy $P_\theta(\theta) \approx 1/2\pi$. The numerical result for that case is fit well by a Gaussian,

$$\overline{\Psi}_s(s) = \sqrt{c/\pi} e^{-cs^2}, \quad |s| \leq 1 \quad (51)$$

with $c = 7.9$. It is shown in Fig. (3) with the fit as the dashed curve. This indicates that in the isotropic case the volume of a grain’s stability space is a Gaussian function of the individual grain’s load-anisotropy, s .

The form of $\overline{\Upsilon}$ depends upon $P_{F\theta}$ and hence can only be found by solving the transport equation.

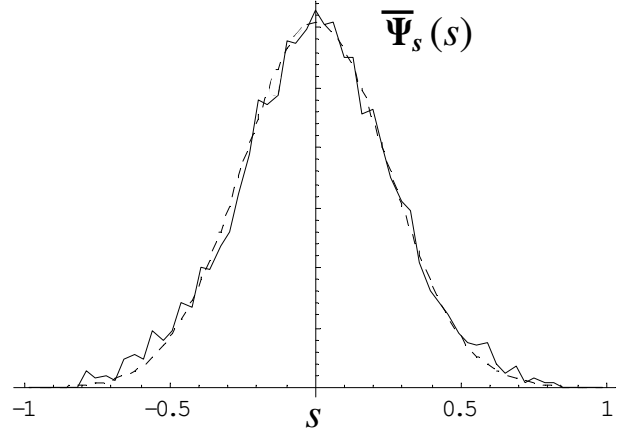


FIG. 3: Grain factor fit to Eq. (51).

H. The Mean Structure Transport Equation

Just as Eq. (27) can be solved recursively, giving us the recursive ‘‘transport’’ equation, so can Eq. (45) be solved recursively, giving us the ‘‘Mean Structure Transport Equation’’ or MSTE.

To develop the MSTE, we convert the load distribution of Eq. (45) into a contact force distribution. This cannot be done simply by collapsing P_{2w} since it does not contain sufficient information. However, the variables may be changed if we first obtain the joint conditional PDF $C_{F\theta}(F, \theta | w_x, w_y)$, so that,

$$P_{F\theta}(F, \theta) = \iint_0^\infty d^2w \ C_{F\theta}(F, \theta | w_x, w_y) P_{2w}(w_x, w_y). \quad (52)$$

This CPDF can be obtained easily through the same change of variables introduced previously, $(w_x, w_y) \rightarrow (s, t)$, because $C_{F\theta}(F, \theta | s, t) = t \cdot C_{F\theta}(tF, \theta | s, 1)$ and the conditional dependency is reducible to the s variable, alone. This may be obtained by straightforward integration,

$$\begin{aligned} C_{F\theta}(F, \theta | s, 1) &= \frac{1}{4} \sum_{i=1}^4 \iiint_0^{2\pi} d^4\theta \ G(\theta_j) \delta(\theta - \theta_i) \\ &\quad \times \delta[F - F_i(s, 1, \theta_1, \dots, \theta_4)] \\ &\quad \times \prod_{k=1}^4 \Theta[F_k(s, 1, \theta_1, \dots, \theta_4)] \end{aligned} \quad (53)$$

where only one term of the sum is needed in many cases due to the symmetries of the ensemble. This reflects the MSA because it assumes that all grains in the same (s, t) mode contribute to the integral according to the same weight. It can be found by very easy Monte Carlo integration, and the result for the case of isotropy, $C_{F\theta}(F, \theta | s, 1) = C_F(F | s, 1)/2\pi$, is shown in Fig. (4).

Combining this CPDF with Eq. (45) and the defini-

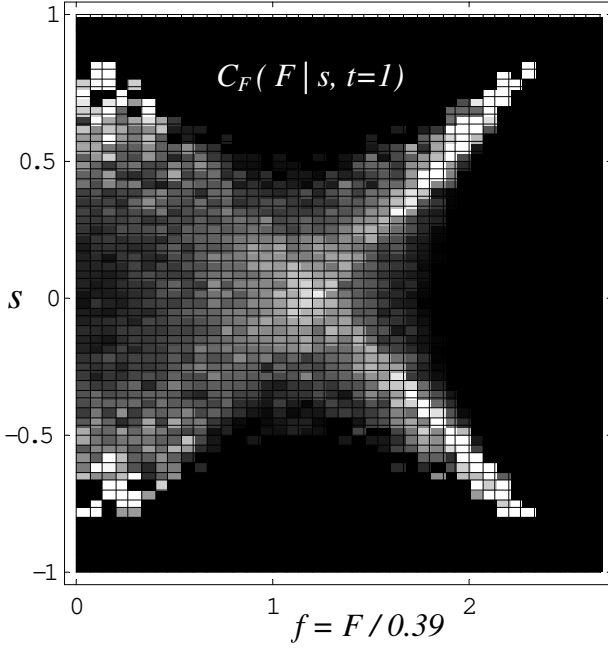


FIG. 4: Horizontal cross sections through this plot are the conditional PDF for f , the normalized contact force magnitudes ($\langle F \rangle = 0.39$ when $t = 1$). White represents higher probability density. The vertical axis represents its dependence upon the s variable with a fixed $t = 1$. Varying t only rescales f .

tions of $C_{F\theta}$, $\overline{\Psi}$ and $\overline{\Upsilon}$,

$$\begin{aligned}
 P_{F\theta}(F, \theta) &= \frac{1}{16\pi^2} \sum_{i=1}^4 \iint_0^\infty d^2w \iiint_0^{2\pi} d^4\theta G(\theta_j) \\
 &\times \delta(\theta - \theta_i) \delta[F - F_i(w_x, w_y, \theta_1, \dots, \theta_4)] \\
 &\times \prod_{k=1}^4 \Theta[F_k(w_x, w_y, \theta_1, \dots, \theta_4)] \\
 &\times e^{-\beta_x w_x - \beta_y w_y} P_{2w}^*(w_x, w_y).
 \end{aligned} \tag{54}$$

$P_{2w}^*(w_x, w_y)$ used in this equation may be obtained a number of ways that should be equivalent within the accuracy of the MSA. Two of these have been used in the numerical results and were shown indeed to produce identical results to within the statistical precision of the data. The first is purely consistent with the MSA, assuming no necessity for *a priori* correlation between the loads and the contact angles. Furthermore, it assumes no *a priori* correlation between w_x and w_y . Correlations arise only after throwing out unstable grain configurations. That is, it assumes a fixed $\overline{\Upsilon}$ over the union of the two ovals in Fig. (2), not just their intersection (the gray region). Imposing $\overline{\Psi}$ then throws out grain configurations outside of the central gray region. This method is,

$$\begin{aligned}
 w_x &= F_1 \cos \theta_1 + F_2 \cos \theta_2, \\
 w_y &= F_3 \sin \theta_3 + F_4 \sin \theta_4
 \end{aligned} \tag{55}$$

(note that all four contacts are treated as if distinctly different despite the fact that an x -hemisphere and a y -hemisphere overlap in one quadrant), and

$$P_{2w}^*(w_x, w_y) = P_{w_x}^*(w_x) P_{w_y}^*(w_y), \tag{56}$$

where

$$\begin{aligned}
 P_{w_x}^*(w_x) &= \iint_0^\infty d^2F \iint_0^{2\pi} d^2\theta \prod_{i=1}^2 P_{F\theta}(F_i, \theta_i) \\
 &\times \delta(w_x - F_1 \cos \theta_1 - F_2 \cos \theta_2),
 \end{aligned} \tag{57}$$

$$\begin{aligned}
 P_{w_y}^*(w_y) &= \iint_0^\infty d^2F \iint_0^{2\pi} d^2\theta \prod_{i=3}^4 P_{F\theta}(F_i, \theta_i) \\
 &\times \delta(w_y - F_3 \sin \theta_3 - F_4 \sin \theta_4).
 \end{aligned} \tag{58}$$

The second method, which will be used in a Monte Carlo solution of the PDFs, attempts greater fidelity to the micromechanics by imposing *a priori* correlation between w_x , w_y and $\{\theta_j\}$. If the MSA is valid, then imposing these correlations should be largely superfluous. Comparing the results of these two methods will therefore test the MSA in Sec. IV.A. The second method, which for simplicity is expressed here for the case of quartered fabric, is

$$\begin{aligned}
 w_x &= F_1 \cos \theta_1 + F_2 \cos \theta_2, \\
 w_y &= F_2 \sin \theta_2 + F_3 \sin \theta_3
 \end{aligned} \tag{59}$$

(note the shared contact \vec{F}_2), and

$$\begin{aligned}
 P_{2w3\theta}^*(w_x, w_y, \theta_j) &= \iiint_0^\infty d^3F \prod_{i=1}^3 P_{F\theta}(F_i, \theta_i) \\
 &\times \delta(w_x - F_1 \cos \theta_1 - F_2 \cos \theta_2) \\
 &\times \delta(w_y - F_2 \sin \theta_2 - F_3 \sin \theta_3).
 \end{aligned} \tag{60}$$

Inserting either of these forms of P_{2w}^* into Eq. (54) produces an MSA recursion equation in $P_{F\theta}$, which is the MSTE. It can be simplified by taking advantage of the various symmetries of the ensemble.

The two different forms of P_{2w}^* produce two different forms of the MSTE. This is striking because one form of P_{2w}^* contains $(P_{F\theta})^3$ whereas the other contains $(P_{F\theta})^4$. The ability of these two very different transport equations to produce the same $P_{F\theta}$ depends upon the validity of the MSA.

III. RESULTS

Here, the following nomenclature is used. The vector magnitude of the contact forces are denoted by F , their distribution is $P_F(F)$, and their mean is $\langle F \rangle$. The corresponding normalized force magnitudes are $f = F / \langle F \rangle$,

which have a distribution $P_f(f) = \langle F \rangle P_F(f \langle F \rangle)$. The Cartesian force components in the x direction are denoted by F_x , their distribution is $P_X(F_x)$, and their mean is $\langle F_x \rangle$. The corresponding normalized Cartesian forces are $f_x = F_x / \langle F_x \rangle$, which have a distribution $P_x(f_x) = \langle F_x \rangle P_X(f_x \langle F_x \rangle)$.

The MSTE in the previous section was solved in a Monte Carlo process for the case of isotropic stress and fabric, with one further simplification. It was found that ξ_x and ξ_y were not exactly zero in the MSA, although they were very tiny ~ 0.01 so that the exponential factors were not exactly unity but were nevertheless negligible. Therefore, rather than implementing the exponential weighting exactly, the forces were simply rescaled with a flat factor in each iteration to prevent incremental growth. This approach is reasonable because the phase space for rigid grains has no inherent force scale, the growth was very small, and the growth was balanced in the x and y components. Hence, the form of the DOS should not be greatly affected by this flat rescaling.

The MSTE was shown to converge efficiently to the same stationary state after beginning from several different initial distributions. The original work was performed with *Mathematica*[®] solving for approximately 5,500 grains. These results are presented in this paper. Ongoing efforts with Fortran demonstrate that converged solutions can be found for a million contacts in about 1 minute on a desktop computer. It is quite easy to obtain data sets of 10^{10} grains or greater, making it possible to study joint or conditional distributions of three or more variables with smooth statistics using only a desktop computer. For some applications this provides a tremendous computational advantage over the fully dynamic simulations.

The $P_f(f)$ resulting from the transport method was shown earlier in Fig. (1). It has all the key characteristics of granular contact force PDFs. A fit, shown as the smooth curve in Fig. (1), was obtained with the form proposed for the data from the carbon-paper experimental method [6],

$$P_f(f) = a(1 - be^{-cf^2})e^{-df}. \quad (61)$$

Using the values $a = 3.28$, $b = 0.85$, $c = 1.56$, and $d = 1.56$, the fit is excellent and is in quantitative agreement with the range of values reported from both experiments and numerical simulations. It should be noted that here, as in most of the empirical distributions [6, 12, 14], d is suspiciously close to $\pi/2$. A plausible reason why this value arises under isotropic conditions is provided in the discussion section.

For the special case of true isotropy in which

$$\begin{aligned} P_{F\theta}(F, \theta) &= P_F(F)P_\theta(\theta) \\ &= P_F(F)/2\pi, \end{aligned} \quad (62)$$

changing variables to Cartesian components $F_x = F \cos \theta$

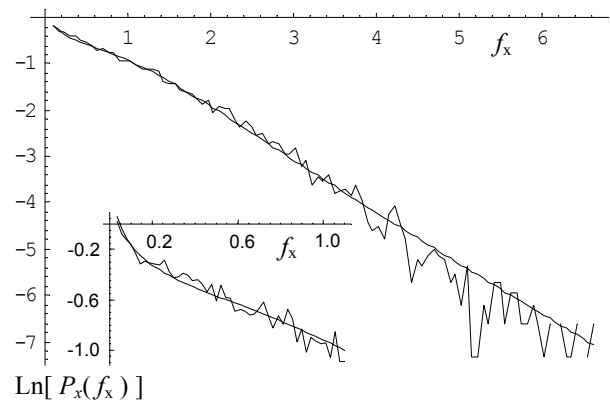


FIG. 5: Semi-logarithmic plot of the PDF $P_x(f_x)$ of the normalized x -components of the granular contact forces $f_x = F_x / \langle F_x \rangle$. The smooth curve was obtained from Eq. (64). The semi logarithmic inset shows the behavior below $f_x = 1$.

is effected in probability theory by the straightforward

$$P_X(F_x) = \int_0^{2\pi} d\theta \int_0^\infty dF \frac{P_F(F)}{2\pi} \delta(F_x - F \cos \theta), \quad (63)$$

or by evaluating the inner integral and expressing as normalized forces,

$$P_x(f_x) = \frac{2 \langle F \rangle}{\pi \langle F_x \rangle} \int_0^{\pi/2} d\theta P_f(f_x \sec \theta) \sec \theta, \quad (64)$$

where the symmetries of isotropy were used to reduce the range of integration in θ . Numerically integrating this [16] with the $P_f(f)$ of Eq. (61) yields the smooth line in Fig. (5). It fits the numerical Cartesian component data from the transport algorithm (shown in the same figure) over the entire range. It has a singularity at $f_x = 0$ and is monotonically decreasing as demonstrated in numerical simulations [15, 16]. It is not purely exponential, the two knees being indicative of a summation of n^{th} order Modified Bessel Functions of the Second Kind, $K_n(\beta_x f_x)$, functions which result naturally when exponential forms are used for $P_f(f)$ in Eq. (64).

The only problem with the fit shown in Fig. (1) occurs in the region of very small forces, $f \lesssim 0.2$. This is the same region in which the form of Eq. (61) could not be experimentally verified due to calibration limits. Therefore it is not known whether this is the correct empirical form in that region [43]. A better fit can be obtained using another form so that it fits excellently over the entire range including $f \ll 1$. This will be accomplished starting with the observation noted above, that the two knees in Fig. (5) are indicative of $K_n(\beta_x f_x)$. These two knees appear very dramatically in a rotation of the coordinates, a rotation which is most easily understood if performed manually by lifting the edge of the page toward the eye and rotating it so that the line of sight is parallel to the segments of the graph in Fig. (5). The fit to $P_f(f)$ will therefore be accomplished by fitting the

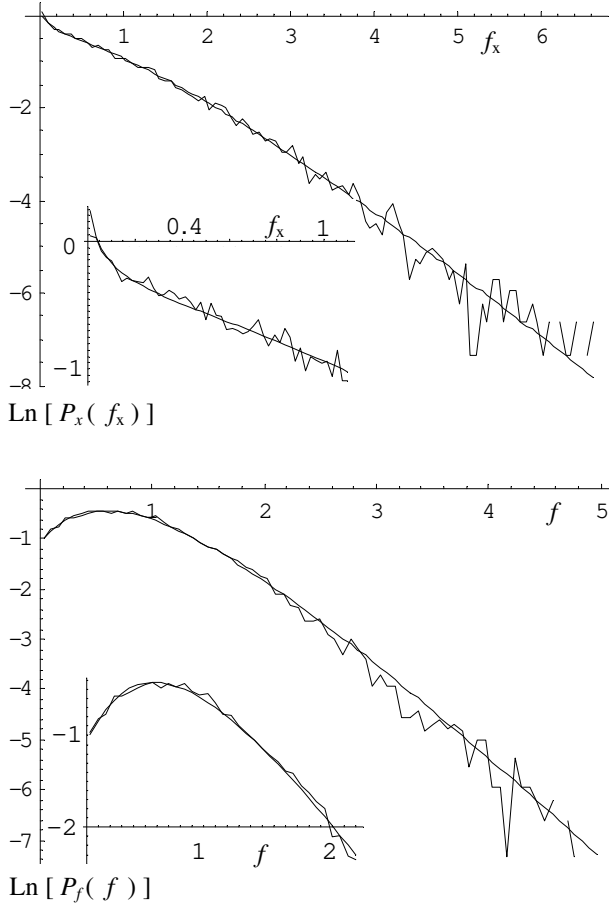


FIG. 6: (Top) The normalized Cartesian force components f_x from the Mean Structure Transport Method fitted to Eq. (65), which appears to be the natural form. The inset shows the behavior below $f_x = 1$. (Bottom) The force magnitudes f from the Mean Structure Transport Method fitted to Eq. (68). The inset shows the behavior below $f = 2$. These two fits analytically transform to one another through Eq. (64) and Eq. (67).

natural forms to $P_x(f_x)$ and then mathematically inverting the transformation of Eq. (64). The simplest fit to within the statistical accuracy of this data set appears to be of the form,

$$P_x(f_x) = C_1 \sum_{n=1}^3 a_n f_x^n K_n(\beta_x f_x) \quad (65)$$

with $a_0 = 6.5$, $a_1 = -12$, $a_2 = 35$, $a_3 = -1$ and $\beta_x = \pi/2$, and where C_1 is for normalization. The fit is excellent over the entire range, displaying all the correct knees and piecewise slopes as shown in Fig. (6)(top). The shape of the knee closest to $f_x = 0$ could be obtained only by including a K_0 term. This term has infinite probability density for $f_x = 0$, but the singularity is very narrow and hence cannot usually be seen in a finite set of empirical data that has been aggregated into bins of finite width [44].

The transformation integral which is the inverse of Eq. (64) cannot be deduced by probability theory because f_x and θ are not statistically independent. Therefore, inverting the change of variables to go from $(f_x, \theta) \rightarrow (f, \theta)$ is not trivial, even in this isotropic case. Nevertheless, the exact relationship can be derived using an approach which is equivalent to the mathematics of X-Ray Tomography [30]. The result is,

$$P_F(F) = \frac{1}{F} \int_0^{\frac{\pi}{2}} d\theta P_X(F \sec \theta) \csc^2 \theta, \quad (66)$$

or, in normalized forces,

$$P_f(f) = \frac{\langle F_x \rangle}{\langle F \rangle} \frac{1}{f} \int_0^{\frac{\pi}{2}} d\theta P_x(f \sec \theta) \csc^2 \theta. \quad (67)$$

This relationship is fascinating because we know that $F_x = F \cos \theta$ and therefore $F_x \leq F$ for all θ ; however, this relationship computes F in terms of $F_x = F \sec \theta$ so that $F_x \geq F$ for all θ . This says that the probability of finding a contact force magnitude F is a weighted sum over the probabilities for all the Cartesian components F_x that are too large to be relevant. Nevertheless it is mathematically correct.

Using Eq. (65) in Eq. (67), we obtain,

$$P_f(f) = \frac{\pi C_2}{2} e^{-\beta f} \sum_{n=0}^3 b_n \langle F \rangle^n f^n \quad (68)$$

with $C_2 = C_1$, $b_0 = a_0$, $b_1 = a_1 + a_2 + a_3$, $b_2 = a_2 + 3a_3$, $b_3 = -a_3$, and $\beta = \beta_x \langle F \rangle / \langle F_x \rangle \approx (\pi/2)^2$. This result fits the numerical data from the MSTE excellently over the entire range of f as shown in Fig. (6)(bottom). It exactly matches the finite and nonzero value of $P_F(0) = \frac{\pi}{2} C_1 a_0$ that occurred in the numerical data, so we see that the a_0 term that made $P_x(f_x \rightarrow 0)$ infinite is the same b_0 term that makes $P_f(0)$ nonzero and finite. The linear plots of Eqs. (65) and (68) are shown in Fig. (7) in order to show that the curve fits are truly good in the region of weak forces, even without the compression of a logarithmic axis.

Fig. (8) shows semi-logarithmically the Cartesian Load PDF $P_w(w)$ produced by the MSTE, computed for several different rotations of the Cartesian axes. These distributions have an exponential tail and a peak near $w \approx 1$. The near similarity of the rotated plots indicates approximate rotational symmetry for this nearly isotropic model, despite its quartered fabric. The variation in the region of weak loads is the result of that quartering. In the unrotated axes, wherein the grains have exactly two contacts on each hemisphere, we find $P_w(w) \rightarrow 0$ as $w \rightarrow 0$. We may fit $P_w(w)$ in these unrotated axes to an exponential with a power law prefactor,

$$P_w(w_x) = \left(\frac{w_x}{\langle w_x \rangle} \right)^\alpha e^{-\beta w_x / \langle w_x \rangle}. \quad (69)$$

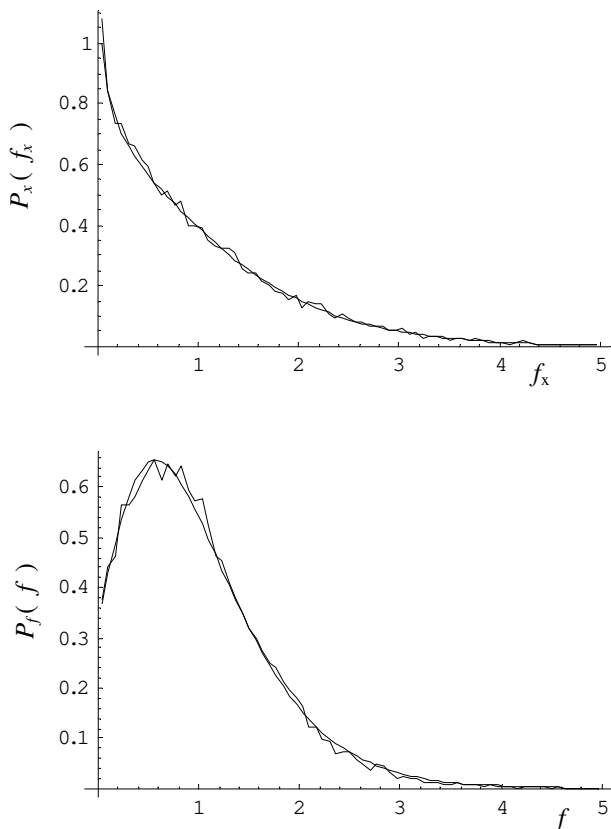


FIG. 7: (Top) Linear plot of the normalized Cartesian force components f_x from the MSTE fitted to Eq. (65). (Bottom) Linear plot of the force magnitudes f from the MSTE fitted

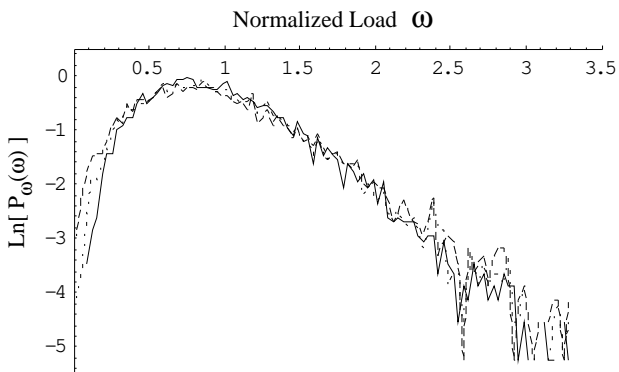


FIG. 8: Semi logarithmic plot of the Cartesian Load PDF, the PDF of the total normalized load borne by each grain in the x or y direction unrotated (solid line), rotated $\pi/6$ radians (dotted line), and $\pi/4$ radians (dashed line).

If the distribution of F_x had been purely exponential and if there had been no correlation between adjacent values of F_x on the same grain, then this should have had values of $\alpha = 1.0$ and $\beta = 1.0$ as in the uniform q model. We do find an excellent fit over the entire curve using this form, but with the parameters $\alpha = 3$ and $\beta = 4$.

By comparison, when the Cartesian axes are rotated

the grains in this model may have 1, 2 or 3 contacts on the sampled hemisphere instead of the strict 2 contacts per hemisphere (1 contact per quadrant) that was defined for the unrotated axes. The $P_w(w)$ for these rotated axes are also shown in Fig. (8). They begin with a *finite* probability density for zero force instead of beginning at zero, and the finite value is maximized when the rotation is $\pi/4$ radians because this is where we obtain the maximum fraction of grains having something other than 2 contacts on the hemisphere. It was found in numerical simulations [15, 16] that when the grains in the bulk are segregated into separate populations having one, two, or three contacts on one side of the grain, respectively, then the Cartesian weight on the grains which support two or three others has a $P_w(w)$ which does go to zero probability for $w \rightarrow 0$. It is the population which supports only one contact which has a nonzero $P_w(w)$ because the load in that case is closely related to $P_f(f)$, which itself is nonzero at zero force. Thus, the MSTE results are in agreement with this aspect of the simulation data, as well.

The distribution of s and t variables resulting from the transport method are fit excellently by

$$P_{st}(s, t) = A \cos\left(\frac{\pi}{2}s\right) \left(\frac{t}{\langle t \rangle}\right)^4 e^{-5t/\langle t \rangle} e^{-7.9s^2}. \quad (70)$$

Thus, by comparing Eqs. (51) and (48) with $\xi_x = \xi_y = 0$, the structure factor can be identified,

$$\begin{aligned} \overline{\Upsilon}_{st}(s, t) &= \cos\left(\frac{\pi}{2}s\right) \left(\frac{t}{\langle t \rangle}\right)^4 e^{-5t/\langle t \rangle} \\ &= \overline{\Upsilon}_s(s) \overline{\Upsilon}_t(t). \end{aligned} \quad (71)$$

$\overline{\Upsilon}_t$ and $\overline{\Upsilon}_s$ resulting from the transport method are shown in Fig. (9) with smooth curves from Eq. (71).

IV. DISCUSSION

The following topics shall be discussed: (1) the validity of the approximations, (2) the relevance of this analysis to the more general cases, the claim being that the frictionless, rigid, round case provides a clearer view into the underlying mathematical structure common to all granular packings, (3) insights that these results provide into the underlying structure of the physics, and (4) several other features of the ensemble which should be noted.

A. Validity of the Approximations

The two approximations which enabled this ensemble analysis are the Assumption of Non-recursive Correlation (ANC) and the Mean Structure Approximation (MSA). Ultimately, the quantitative validation of these requires a careful comparison with numerical simulation data for

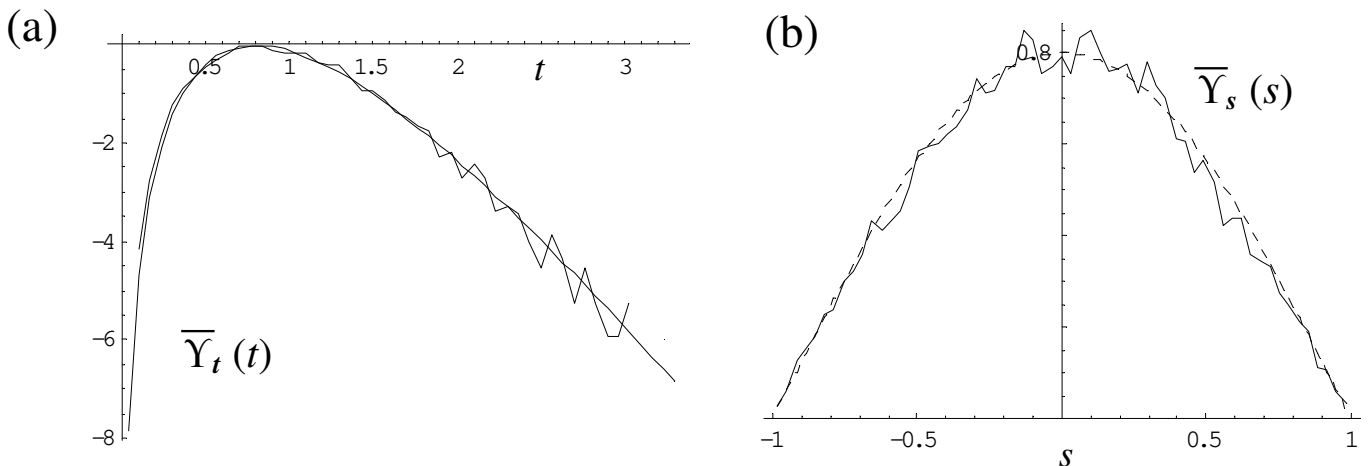


FIG. 9: Structure factor obtained from the Mean Structure Transport Method, fit to Eq. (71) for the case of isotropy with $\langle w_x \rangle = \langle w_y \rangle = \langle t \rangle / 2 = 1/2$, (a) semilog plot of t -dependence, (b) linear plot of s -dependence.

particular states of the stress, fabric, and rheological history, and this has not yet been performed. Meanwhile, the quantitative validity of the approximations is already evident to some degree, as discussed below.

1. Validity of the ANC

If correct, the validity and usefulness of the ANC is the most important and fundamental piece of new physics presented in this paper because it provides a way to solve some relevant aspects of the statistical mechanics of static granular packings.

Note that beside the constraints which defined the ensemble's DOS in Eq. (2) or (8), another geometric constraint is needed to ensure closure of every “loop” of grains in a packing. Without this closure, the chains of contacting grains are allowed to branch out ever increasingly in all directions and overlap into one another's space. Geometrically, then, omitting this constraint does not produce a good approximation to a packing. However, it should be an excellent approximation as far as the statistics of single-grain states are concerned.

It has been shown [14] that contact forces on the same grain are strongly correlated with one another. There is anti-correlation for contacts closer together than $\Delta\theta \approx 0.4\pi$ radians of angular separation, and a positive correlation when the angular separation is greater than that. The correlation continues to increase as the contacts are increasingly distant from one another but still on the same grain. The correlation dramatically drops immediately thereafter when the distance between contacts becomes greater than one grain diameter.

The strong intra-grain relationships make sense due to the requirements of static equilibrium of the individual grains. Contacts on the same quadrant compete for a share of the same load and hence are anti-correlated. Contacts opposite one another transmit load through one

another and hence are correlated. Similistically we could expect $\Delta\theta = \pi/2$ to be the crossover point of no correlation as illustrated in Fig. (10). This is approximately correct, and the error is probably attributable to the existence of three-grain loops, history-dependent frictional effects, and so on.

Likewise, the sudden drop in correlation after one grain diameter of separation is also understandable in terms of the local mechanics. It is true that neighboring grains share a common contact so that contacts on adjacent grains are just two sequential two-point correlations away from one another. This induces correlations between them. However, these inter-grain correlations should be primarily the result of the information contained in the sequential two-point intra-grain correlations because the lack of cohesion makes the grains otherwise (largely) independent. Additional constraints are not found in the packing until entirely closed loops of grains are considered so that the sequential two-point correlations come all the way around the loop back to the original grain, again. In 2D the typical closed loop consists of four grains, each grain being a vertex between a pair of contacts that form the loop. The four-point correlation constructed as three sequential two-point correlations going the long way around a loop would undoubtedly be very weak compared to the single two-point correlation going the short way around the same loop, since the short way is intra-grain. Fig. (10) illustrates this statement. Hence, the extra correlation information imposed going the long-way around the loop must be very weak compared to the information already present intra-grain. It should therefore be an excellent approximation to neglect this additional information and consider only the intra-grain relationships in defining the DOS. This is the “Assumption of Non-recursive Correlation,” or ANC.

This is not a rigorous argument because we should consider the sum of information from *all* the loops in the packing that contain the grain in question, and it is con-

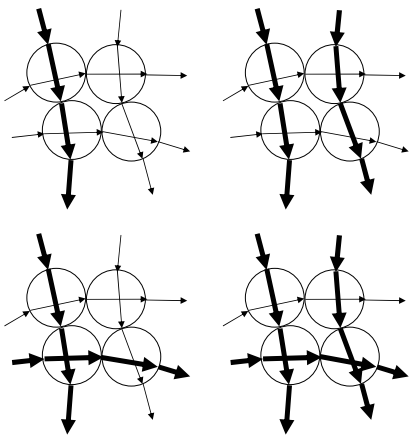


FIG. 10: Contacts that are approximately $\pi/2$ radians away from one another on the same grain are only weakly correlated as illustrated by the closed loop of four grains that allows any combination of weak and strong force chains to pass through it. If the angles were precisely $\pi/2$, then the four force chains in this figure would be completely independent.

ceivable that the sum of very many weak contributions may be strong. However, due to the randomness of the packing, and the large number of amorphous packings that may exist in the configuration space, it is expected that the contributions from increasingly larger loops of grains will be increasingly decoherent and largely cancel one another. Hence, there is good reason to assume that only the intra-grain contribution to the correlations is significant in agreement with the ANC.

If correct, the ANC is an important statement of the physics because it fundamentally characterizes the DOS and provides deep insight into the organization of the physics. In contrast to thermal systems, with granular packings it would be completely unsatisfactory to use a mean-field approximation because this would throw away the structure resulting from the strong two-point correlations (remembering that these have been observed empirically). However, by including only this next higher level in the approximation, that is, only the two-point correlations (and assuming that higher correlations exist strictly as a sequence of two-point correlations) the maximization of a state-counting entropy and the solution of the resulting transport equation produces excellent results as shown in the previous Sec. III. The two-point correlations therefore appear to be the essence of the physics. Further work is needed to carefully test this hypothesis.

2. Validity of the MSA

The MSA is important because, if correct, it characterizes the structure factor as being a functional of $P_{2w}^*(w_x, w_y)$ rather than $P_{F\theta}(F, \theta)$, and this offers the possibility to decouple the fabric from the force distributions in a way that will help the development of a full theory of rheology. In the meantime, pending rigorous

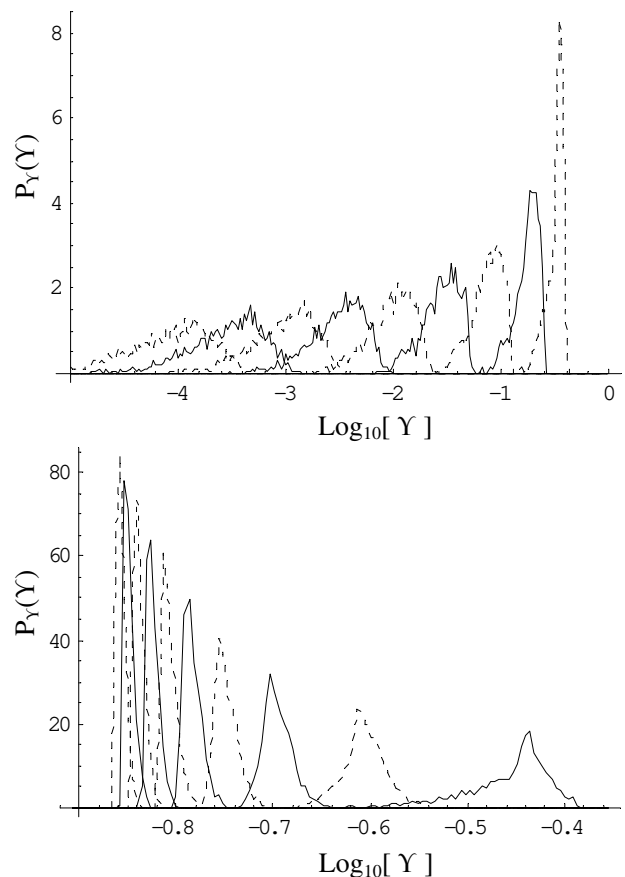


FIG. 11: Distribution of values of $\Upsilon(s, t, \theta_j)$ for fixed value $s = 0$ and several fixed values of t . (Top) From left to right, $t = 10$ (dashed), 9 (solid), 8 (dashed), 7 (solid), 6 (dashed), 5 (solid), 4 (dashed), 3 (solid), and 2 (dashed). (Bottom) From left to right, $t = 1/10$ (dashed), $1/9$ (solid), $1/8$ (dashed), $1/7$ (solid), $1/6$ (dashed), $1/5$ (solid), $1/4$ (dashed), $1/3$ (solid), $1/2$ (dashed), and 1 (solid).

testing of the MSA, the following three considerations are presented to help justify it.

First, the results produced by the MSA appear to be in excellent agreement with the numerical simulation data. A focused effort is needed to further test the limits of the quantitative agreement for specific cases of stress and fabric.

Second, the values of Υ have been calculated according to Eq. (10) for the data obtained in the MSTE. The CPDF $P_\Upsilon(\Upsilon | s, t)$ was calculated for various fixed values of s and t and these are presented in Figs. (11) and (12) for $s = 0$ and $s = 0.6$, respectively. For some values of s and t , the ratio $\Upsilon^{(\max)}/\bar{\Upsilon}$ is as high as 3 (or greater) and $\Upsilon^{(\min)}/\bar{\Upsilon}$ is as small as $1/3$ (or lower). This means that some grain configurations $\{s_i, t_i, \theta_{ij}\}$ will occur three times too often or only $1/3$ often enough in the MSA ensemble compared to the exact Edwards ensemble. This effect is most pronounced when t is high and s is low. However, high values of t are rare to begin with. Furthermore, the distribution for each pair of values for

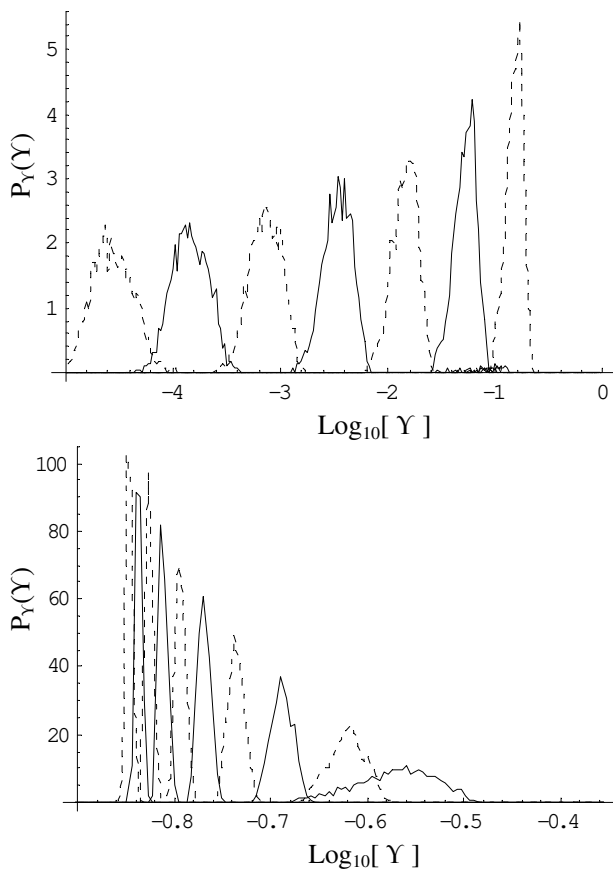


FIG. 12: Distribution of values of $\Upsilon(s, t, \theta_j)$ for fixed value $s = 0.6$ and several fixed values of t . (Top) From left to right, $t = 8$ (dashed), 7 (solid), 6 (dashed), 5 (solid), 4 (dashed), 3 (solid), and 2 (dashed). (Bottom) From left to right, $t = 1/10$ (dashed), $1/9$ (solid), $1/8$ (dashed), $1/7$ (solid), $1/6$ (dashed), $1/5$ (solid), $1/4$ (dashed), $1/3$ (solid), $1/2$ (dashed), and 1 (solid).

(s, t) is localized with a clear peak and so the majority of grain configurations will have a value of Υ that is *relatively* not very far from $\bar{\Upsilon}$ while being distinctly separate from the $\bar{\Upsilon}$ for other values of (s, t) . These latter considerations imply that the MSA does characterize the organization in the DOS qualitatively, but more effort is needed to show whether it is quantitatively sufficient.

Third, two different sampling schemes were implemented as presented in Eqs. (58) and (60). The results were identical to within the statistical precision of the data, as shown in Fig. (13). This supports the MSA because it shows that the resulting distributions are insensitive to the existence or non-existence of correlations between the Cartesian loads and the contact angles, and this is the essence of the MSA.

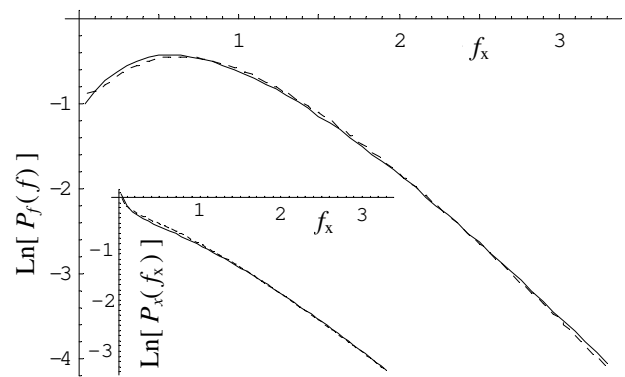


FIG. 13: Comparison of the $P_f(f)$ (large plot) and $P_x(f_x)$ (inset) that resulted from the mean structure transport method using two different sampling methods. In each plot the solid line uses sampling as Eq. (58) with quartered fabric, whereas the dashed line used sampling as in Eq. (60) but with non-quartered fabric. The results are statistically indistinguishable, lending credence to the mean structure approximation.

B. The Priority of the Frictionless Ensemble

The empirical data show that the PDF of contact force magnitudes (or normal components) have the same qualitative form in frictional and in frictionless packings. In their physical and mathematical structure, however, it appears that frictionless packings are the more fundamental case and therefore serve better to elucidate the organization of the physics. There are several reasons to make this claim, including considerations of phase space, imposed correlations, contact nonlinearity, isostacy, and perturbational relationships. These are not five independent arguments, but overlap one another and in the final analysis will probably be known as different ways of saying the same thing. Nevertheless, since the complete understanding of granular matter has yet to emerge, they are presented as five snapshots to help build the argument.

1. Heirarchy of Phase Space Axes

This paper has shown that Edwards' flat measure with frictionless grains produces the correct forms of the PDFs. By way of contrast, Kruyt and Rothenburg have presented an entropy maximization approach to *frictional* granular materials which implicitly assumes that the accessible region of the phase space is uniformly occupied for all sets of contact forces, both normal and frictional forces at each contact, without enforcing N2L at the individual grains [3]. The chief difficulty to the method is that it omits the physics that would have produced the grain and structure factors. Nevertheless, it provides important insights including one critical observation regarding the nature of frictional forces. It assumes that

the accessible region of phase space is shaped (in part) by the Coulomb friction law. That is, the normal and tangential force components at each contact, F_n and F_t respectively, obey the Coulomb friction law $|F_t| \leq \mu F_n$, where μ is the static coefficient of friction. This causes the projection of the accessible region of phase space onto the (F_{ni}, F_{ti}) plane (representing the i^{th} contact) to take the shape of a wedge centered on the F_n axis with its vertex on the origin and having a half-angle of $\arctan \mu$. As a result, the accessible volume of phase space vanishes for $F_n \rightarrow 0$ for this or any other contact. Therefore, if the DOS is subject to Coulomb friction with a flat measure then by necessity $P_F(F \rightarrow 0) \rightarrow 0$, which indeed the method predicted. This, however, contradicts the empirical evidence both in experiments and in numerical simulations.

This demonstrates that Edward’s hypothesis cannot be taken to mean that every metastable force state is equally probable. Rather, it can only mean that every metastable *geometry* is equally probable. Otherwise, the observed $P_F(0) > 0$ in simulations with friction would invalidate the hypothesis. Hence, it is necessary to impose a hierarchy among the phase space axes. The DOS may be uniform across the accessible region of the *normal* force axes (which therefore play the more fundamental role), but the DOS cannot be uniform across the accessible region of the *frictional* force axes (which therefore play a secondary role). Therefore, it is of first importance to understand the distribution of states across the normal axes, being the more fundamental and applicable to both the frictional and the frictionless packings. Later it will be important to understand the perturbations that result when the frictional degrees of freedom are joined onto the phase space.

2. Hierarchy of Imposed Correlations

The force conservation laws are a primary organizational feature of the ensemble, and the extension of layers corresponding to each of these conservation laws is orthogonal to each of the others so that they intersect in just a single grain, usually just a single contact. The way that the several Cartesian components are related to one another at the individual contacts is therefore what determines how the orthogonal conservation laws interact and affect one another. This means of interaction between the conservation laws is a uniquely granular feature. In other types of solids, or when granular physics has been coarse-grained to identify the macroscopic properties, the interactions are described by solid continuum mechanics and are of a completely different character. Therefore, it is fundamentally important to examine the relationship of Cartesian components at the individual contacts.

In all cases the Cartesian components are correlated through the contact angle, and the degree of correlation is dependent upon the degree of friction and cohesion.

Cohesionless, frictionless packings are the most correlating because a force vector can lie only in the contact direction pointing inwardly. Coulomb friction spreads that ray into a cone, and perfect friction opens the cone to encompass the entire hemisphere. Imperfect cohesion further reduces the organization because the force vectors can point anywhere in the entire sphere, but asymmetrically with respect to the tensile and compressive hemispheres. Finally, perfect cohesion with perfect friction produces the least organization of all because it removes all correlation between the Cartesian components, and thus it is no longer a granular packing.

The essence of granular packings is the fragility, which organizes the force state so that the Cartesian components are correlated through the contact angles, thereby resulting in the uniquely granular interaction of orthogonal conservation laws. By contrast with the non-granular case, the “most purely granular” system, the one at the top of this friction/cohesion hierarchy, is the cohesionless, frictionless case. Friction tends to obscure the things that are inherently granular.

3. Contact Nonlinearity

In a packing of cohesionless grains there is an inherent non-linearity associated with normal force vectors because when perturbed they cannot reverse direction from compression to tension. This non-linearity does not exist with tangential (frictional) force vectors because they can reverse direction smoothly when perturbed. Hence, the distribution of normal forces is one-sided and discontinuous at $F = 0$ (the famous $P_F(0) > 0$), whereas the distribution of frictional forces is two-sided and continuous. The normal force non-linearity produces the grains’ ability to tip and form new contacts, and this is the quintessential fragility that makes granular materials granular [28]. Thus once again, the normal components are fundamentally related to the essential behaviors and the frictional forces are not.

4. Isostacy

Frictionless packings are isostatic whereas frictional packings are hyperstatic [22, 37]. Therefore, the contact nonlinearity described above functions in a frictionless packing to self-organize the contact network, maintaining exactly the same number of contact forces (unknowns) as there are mechanical degrees of freedom (equations). In frictional packings, on the other hand, this special behavior is lost and the number of contacts becomes variable. In this light, the presence of friction can be seen as a spoiling influence that obstructs the self-organizing behavior. In order to explain how the spoiling occurs it is necessary to understand the more fundamental behavior that is being spoiled.

5. Perturbational Relationships

Finally, in some cases (at least) the frictional degrees of freedom can be understood as a perturbation frozen into an underlying frictionless solution. Starting with a static frictionless packing, the rigid grain contact law of a frictionless packing can be replaced by springs which can support compression but pull away from the grains instead of providing tension. Vibrations induced into the network can be frozen into the packing by suddenly “turning on” friction. This picture makes several predictions that appear to be in good agreement with the empirical data. If the frictional case is indeed a perturbation of the frictionless case, then it is obvious that the frictionless case must be studied and explained first because it is the more fundamental.

6. Summary: Relevance of the Idealized Ensemble

Most granular media in nature, such as sand, are highly frictional. However, the frictionless case is important for two reasons. First, some important static “granular packings” are indeed frictionless. These include emulsions [19], monatomic liquids quenched beneath the glass transition [9], and (approximately frictionless) smooth balls in some industrial applications. Second, and more importantly, it serves to elucidate the underlying and more fundamental organization that exists even in frictional granular packings as discussed above. The present analysis considers the inclusion of friction to be an important but necessarily future generalization, and so for now priority is given to frictionless packings.

Likewise, perfectly cohesionless grains represent the more idealized case because the opposite—when there is perfect cohesion—is no longer a case of granular physics at all. The use of non-round grains is in one way similar to the use of frictional grains because it provides a mechanism for torques to appear on the grains, introducing N rotational degrees of freedom to the packing of N grains. Perfect grain rigidity is also the more idealized case because it renders the form of the contact work function irrelevant so that $P_f(f)$ takes on the universal form [38]. Also, imperfect rigidity induces non-roundness which enables the torquing of grains. Keeping with the idealized frictionless case, then, this analysis focused on the related round and rigid idealizations in order to elucidate the physics without those degrees of freedom. All these idealizations have been shown in numerical simulations to produce the same qualitative features as the more generalized cases and hence the ensemble is not too idealized to explain the fundamentals of their statistical physics.

C. Insights into the Physics

1. Exponential Tail

The exponential tail reflects maximum entropy in the presence of a conservation law, as usual. In fact there are two conservation laws in a 2D packing, but in frictionless packings each contact can compete for a quantity of the force that is conserved in the sequence of layers that is *normal* to itself; it cannot compete for any part of the force that is conserved in the sequence of layers *orthogonal* to itself. Therefore, rotating the stress tensor into the direction of each individual contact scales the conservation law relative to that particular contact. The distribution $P_f(f)$ represents the accumulation of data from all orientations, but in the case of isotropy all orientations are similar so all contacts form the same statistical mode with the same decay constant, which turns out to be $\beta \approx \langle F \rangle / \langle F_x \rangle \approx \pi/2$.

This value for β is reasonable because the magnitude of each normal force \vec{F} competes for a share of the total force contained in whatever layer of grains is normal to its own contact orientation whereas most of the other contacts supporting that same layer are not normal to the layer. That is, a contact does not compete against other vector magnitudes for a share of the available loads; it competes against Cartesian components that are parallel to itself.

For example, if we assume that the Cartesian components in that orientation have a distribution that is approximately Canonical,

$$P_X(F_x) \approx \beta_x^{-1} e^{-\beta_x F_x}, \quad (72)$$

where $\beta_x^{-1} = \langle F_x \rangle$, then by Eq. (67) we find

$$P_F(F) \approx \langle F_x \rangle^{-2} F K_0(F / \langle F_x \rangle), \quad (73)$$

where K_0 is the zeroth-order Modified Bessel Function of the Second Kind. The mean value of force is therefore

$$\begin{aligned} \langle F \rangle &\approx \langle F_x \rangle^{-2} \int_0^\infty F^2 K_0(F / \langle F_x \rangle) dF \\ &= \frac{\pi}{2} \langle F_x \rangle, \end{aligned} \quad (74)$$

so that,

$$P_f(f) \approx f K_0\left(\frac{\pi}{2} f\right). \quad (75)$$

The asymptotic behavior of this function for large f is

$$P_f(f) \sim e^{-(\pi/2)f} \approx e^{-1.6f}, \quad (76)$$

which is in excellent agreement with the simulation and experiment data. Indeed, $P_x(f_x)$ is approximately Canonical over the region of experimental interest as seen in Fig. (5) in which the data stay very close to a straight line of slope $-\beta_x = -1$.

The decay constant obtained with the form Eq. (68) was quite different than the one obtained using the form Eq. (61), $(\pi/2)^2$ versus $\pi/2$, although both forms provide a good fit to the tail over the range of experimental interest $3 < f < 6$. It turns out that the asymptotic slope of Eq. (68) does not appear on a semi-logarithmic plot until approx $f > 11$. It would take on the order of 10^{13} grains to obtain a flat-line fit over the range $11 < f < 15$. Therefore, slopes fitted to the range of experimental interest are not the true asymptotic slope and may be expected to vary significantly from one simulation study to the next depending upon the form in the region of weak forces, which varies strongly with the stress and fabric anisotropy. This may explain some of the variability of the exponential decay constant in the published studies.

2. Bessel versus Exponential Forms

It turns out that $P_x(f_x)$ is not truly Canonical, but only approximately so over the range of experimental interest. According to the transform pair Eqs. (64) and (67), if $P_x(f_x)$ has an exponential form, then $P_f(f)$ must have a Modified Bessel form, and *vice versa*. So the question is, which one of these distributions has an exponential form (predicted by the binomial counting of an entropy maximization approach), if either of them? The transport method indicates that it is $P_f(f)$ that has the exponential term (with a polynomial prefactor), whereas $P_x(f_x)$ is a summation of Modified Bessel Functions of the Second Kind. Thus it appears that the more uniform DOS occurs in a phase space defined by the normal components, not by the Cartesian components. This makes sense physically because the individual Cartesian components cannot respond independently to the reservoirs of force contained in the sequence of layers normal to themselves, but instead must remain correlated through the contact angle to the other Cartesian components at the same contact. For the case of frictionless grains this correlation is absolute. For grains with Coulomb or another imperfect friction law the correlation is weakened but still present. In either case, the Cartesian phase space must be populated according to these correlations which prevent uniformity in the DOS. The normal force phase space does not have this additional constraint on its DOS. Any change in force at the contact is simply seen as the normal force responding to the reservoir contained in the sequence of layers normal that one contact, whatever that orientation may be. Hence, $P_x(f_x)$ has the Modified Bessel form and $P_f(f)$ has the exponential form with a prefactor.

3. Bias Against Weak Forces

The two items above indicate that $P_f(f)$ would have been Canonical (no prefactor) had the reservoir of force been a truly thermal reservoir. However $P_f(f)$ is not

a monotonically decreasing form, but has a peak near the average force and a less-than-exponential probability density for forces below the average force. In other words, the DOS discriminates against weak normal forces. It is tempting to compare this to the MB velocity distribution which also has a peak and an increasing power law for weak particle velocities. However, this would not be correct as the velocity distribution depends upon the independence of the Cartesian components, an independence which is absent here. Instead, the simple explanation is that the force reservoir is not thermal but instead has strong, localized structure in the immediate vicinity of each contact. This structure is of course the grain itself. Each contact must share a grain with a small, nearly predictable number of other contacts, distributed fairly evenly on the grain due to steric exclusion, and together these contacts must satisfy detailed balance in each spatial dimension. This results in correlations between the neighboring contacts. Thus, weak forces find fewer ways to exist on a stable grain than do the stronger forces because they are closer to the non-linear “cliff” (the non-allowance of tensile forces) and it does not take as much perturbation of the local correlative structure to push them over that cliff. Hence, there is a reduced volume of stable configuration space for grains which have one or more weak forces. This was proven analytically for a special illustrative case in Ref. (38).

Referring again to the analogy with a dilute classical gas, the time which the particles spend in collisions is small and is usually ignored, and it is usually assumed that the DOS in the accessible region of phase space is uniform as motivated by several considerations. This is in contrast to granular packings in which every “particle” (i.e., grain contact) has its entire existence shared by two “collisions” (grains) with no trajectory between them. Thus, the DOS is entirely defined by the set of allowable collisions. The peak in $P_f(f)$ is the result of the dynamic process before the ensemble of metastable states came into existence. In that process stable grain configurations are kept and unstable configurations are dynamically rejected until a highly-ordered stable configuration is achieved, thus denuding an otherwise canonical distribution in the region of its weaker forces. Therefore these features do not result from the maximization of the entropy *per se*, but due to the self-organization that keeps entropy small.

4. The Importance of Edwards’ Hypothesis

This analysis has shown that Edwards hypothesis, the assumption that every metastable state is equally probable, is sufficient to produce the correct forms for the PDFs. We did not know beforehand whether this would be the case. It is possible that the configuration space is not equally accessed by the dynamic process that self-organizes the packing. The final DOS might have displayed dominant features that are attributable to the

dynamics rather than to the topology of the space and then the form of the PDF would have reflected those features. However, this analysis has shown that Edwards’ flat measure alone produces the correct PDFs. (Edwards’ hypothesis has also been tested dynamically in regard to the fluctuation dissipation theorem [39].) Further testing is needed to determine whether the dynamics may be completely decoupled from all the relevant statistics in quasi-static rheology. If so, then it may be possible to develop a quasi-static rheological theory using a small set of simplistic assumptions based on Edwards’ hypothesis. This would be analogous to the case of classical thermal systems near equilibrium, where the kinetic theory has been decoupled from the statistical mechanics to excellent approximation by using a small set of simplistic assumptions.

5. Temperature as a Second-Order Tensor

An interesting observation arises in the analogy to thermal systems. While thermal systems possess several conserved quantities, only one of them—energy—is conserved with respect to its *own* conjugate dimension—time. (The linear and angular momenta are not conjugate to time.) Temperature is the intensive scalar corresponding to that unique conservation, scaling the exponential decay of the energy distribution. In 3D granular packings there are three extensive quantities each conserved with respect to its own conjugate dimension. The stress *tensor* is the corresponding intensive object: it scales the several conservation laws and also defines the orientation of their conjugate spatial dimensions. (This use of the stress tensor as a second-order tensorial temperature first appeared in Kruyt and Rothenburg’s method [3] in the form of a Lagrange multiplier.) Thus, granular statistical mechanics might be viewed as a tensorial generalization of scalar statistical mechanics.

Because of this generalization, $P_F(F)$ is not a sufficiently general analogy to the energy distributions of thermal systems. Sufficient expressions for 2D frictionless packings include $P_{2\xi}(F_x, F_y)$, which is the JPDF of Cartesian components aligned along the principle stress axes, or $C_F(F | \theta)$ which is the CPDF of contact force magnitudes as a function of their corresponding contact directions. By the strength of the tensorial analogy we can expect that the two principle elements of the stress tensor (in 2D) will scale the exponential decay of either of these PDFs in the corresponding two principle directions. Except for the isotropic case, collapsing these to $P_F(F)$ represents a loss of information and obscures the organization of the physics.

6. Choice of the Phase Space

In the absence of tangential forces or cohesion, it is the set of normal forces grouped for individual grain stabil-

ities that become the relevant descriptor of the physics. However, one might argue that a Cartesian phase space may be equally relevant because: (1) in a homogeneous test cell the stress tensor is translationally invariant (vanishing fluctuations in a volumetric average in the thermodynamic limit) when expressed in Cartesian coordinates, (2) corresponding to this fact, the extensive version of the force conservation laws are organized in Cartesian layers, and (3) the stress tensor is diagonalizable for a particular rotation of the axes thus implying a preferred orientation of those Cartesian layers. However, the fragile granularity of the medium wherein those conservation laws interact makes them tensorially-related instead of independent from one another. Rotation of the tensor describes the quantity of force competitively available to each contact. The frictionless contact law ensures that shear in a particular rotation of the tensor is irrelevant to the individual contact. The individual grains have no knowledge whether such an orientation of the tensor is diagonalized. Thus, all the physics is localized to the individual grain in its own polar coordinates. This argues the plausibility of Edwards’ flat measure in \mathbb{S}_2 as opposed to \mathbb{S}_3 where the non-flat Jacobian was included.

7. Fabric Evolution and Chemical Potential

The ultimate goal is to develop a first-principles theory that predicts the rheological evolution of the fabric (including the compactivity) under incremental changes of the externally-applied stress state. It can be expected that the most probable fabric to occur in an ensemble undergoing quasi-static rheology should represent the vast majority of packings in the ensemble when the number of grains is extremely large, and in that sense it becomes statistically deterministic in all of its relevant features. In the much simpler, present analysis of static packings (no rheology), we hope to lay the groundwork for a quasi-static theory. Hence, relying upon the statistically deterministic relationship with fabric in the thermodynamic limit, it is meaningful to decouple the evolution of fabric from the distribution of forces and simply specify the fabric instead, in the same way that scalar compactivity may be specified in Edwards’ ensemble. The fabric distribution $J_{4\theta}(\theta_1, \dots, \theta_4)$ is therefore used to specify the regions of phase space that are uniformly populated.

It should be noted, however, that anisotropic compaction plays a role that may be analogous to chemical potential rather than to temperature. The set of all contacts existing at a specified orientation may be considered a distinct thermodynamic “mode” (similar to the concept in Ref. 3). The isostacy of frictionless packings requires that as one mode loses particles then other modes must gain them, so the total number of particles is conserved. Most of these modes exchange “energy” (total force) with one another, too, because they are not orthogonal. Developing a static theory of granular packings into a rheological theory might therefore be analogous to the general-

ization from Canonical to Grand Canonical. The present analysis aims to explain how forces distribute among the modes when the distribution of particles is specified; a rheological theory would explain how both the forces and particles distribute among the modes. The fabric tensor or some form of generalized compactivity may therefore play the role of chemical potential, regulating the probability of particle exchange between modes during the rheology.

V. SUMMARY AND CONCLUSIONS

This analysis has identified the ANC as a physically-meaningful statement of the behavior of forces in static granular media. Further testing is needed to validate that statement. The use of the ANC makes it possible to solve the DOS based upon Edwards' flat measure in a frictionless granular packing with localized isostacy. This produces a transport equation that can be solved (at least numerically). It was argued that the frictionless case is the one which presents the uniquely granular organization of the physics in its pure form. Solution of this transport equation in the MSA was shown to produce the correct features for the contact force distributions.

This success tends to validate Edwards' hypothesis: the DOS appears to be dominated by features inherent to the static phase space, depending solely upon the packing's present fabric and the stress tensor. That is, the DOS may not be shaped too significantly during the physics of the dynamic regime before the packings achieve static equilibrium. If this is confirmed in other tests, then the importance of it could hardly be overstated: it would statistically decouple the statics from the dynamics and thereby offer the potential to develop a statistical mechanics theory of rheology.

The need for further work is apparent. First, the two approximations have not been adequately validated. The quantitative results should be compared against dynamic simulations of rigid, frictionless grains with carefully controlled stress states and carefully measured fabric, something that has not yet been performed because most studies have either included gravity or not reported the stress state or fabric.

Second, the analysis should be extended and numerical results presented for more general cases. If successful, the case with anisotropic stresses and fabric should demonstrate the qualitative evolution of the PDFs under shearing. This work has begun, and the initial results are hopeful. Extending the analysis to the isostatic 3D case should be relatively easy and after doing so the qualitative differences between 2D and 3D packings should be compared against those noted in the published literature. Also, extension to delocalized isostacy may not be too hard, examining units of greater than one grain at a time or by using other techniques. The effects of delocalized isostacy can also be studied in numerical simulation by segregating the grains into populations having differ-

ent coordination numbers and comparing the PDFs and other statistics for each population. This sort of numerical study would also be crucial to guiding the generalization of the method into delocalized isostacy.

Third, the forms of the functions that fit the numerical data for $P_{st}(s, t)$ are tantalizingly simple and imply the existence of a more basic structure in the physics than has been exposed thus far. This strongly hints at a simple, underlying structure and implies that a more elegant explanation of the physics should be possible. In fact, if the cause of this structure can be identified then a completely analytical solution to the entire problem should be possible (at least to within the ANC and MSA with localized isostacy).

Fourth, solution of the transport equation without the MSA is being developed. Those results compared against the present study will be an important test of the MSA.

Finally, the idea that quasi-static fabric evolution may be predictable through the use of a generalized chemical potential deserves further exploration.

Acknowledgments

I am grateful for helpful discussions with Aniket Bhattacharya of the University of Central Florida Physics Department and with Robert Youngquist of NASA's John F. Kennedy Space Center.

APPENDIX A: THE SHAPE OF THE DISTRIBUTION

1. Peak Near the Average Value of Force

The small peak near the average value of force $F = \langle F \rangle$ has been questioned because some studies show instead a plateau at weak forces or even a monotonically decreasing form of $P_F(F)$ with only a sudden change in slope near $F = \langle F \rangle$. However, it has been shown that these form variants smoothly evolve from one to another as a function of the anisotropy of the stress state and fabric [5, 17]. Also, residual kinetic energy can produce a similar evolution of forms [9], and it is possible that frictional grains may behave somewhat differently than frictionless ones in the region of weak forces [14] depending upon the friction law and history of construction or rheology. These considerations are sufficient to explain all the published variations in the form of $P_F(F)$ and in many cases to qualitatively predict the form.

2. Non-zero Probability Density at Zero Force

The Simplest Model of Edwards and Grinev [2] produces $P_F(F) \rightarrow 0$ as $F \rightarrow 0$, but with a very steeply rising power law to the peak. The slope $P_F'(F)$ is so large that statistically aggregating the predicted $P_F(F)$ into bins

$F_i = (i-1/2)\Delta F$ of width ΔF , as is done in the empirical studies, would put the numerical value of the bin closest to zero force at a value $\sim (dP_F(F)/dF) \cdot \Delta F/2$, which may be significantly greater than zero. This would give the *false* appearance of $P_F(0) > 0$ for the unaggregated data, which seems to explain the observed non-zero value at zero force as a numerical artifact. This explanation, however, would not be correct. First, the form of $P_F(F)$ smoothly evolves under increasing anisotropy to become a monotonically decreasing function [5, 17], and this evolution cannot be plausibly explained unless the non-zero value is real. Second, Edwards and Grinev's model unrealistically implies that every contact on a grain will receive non-negative contributions of force from each of the other contacts so that no contact tends to lift the grain up and away from any of the others. Thus the model has no provision for grain tipping, which explains the predicted shortage of contacts carrying nearly zero force at the threshold of tipping. Third, the present analysis explains that the non-zero value at zero force is a necessary characteristic of the accessible region of phase space, predicted by Edward's flat measure.

As discussed in this paper, the method by Kruyt and Rothenburg [3] also produces a $P_F(F) \rightarrow 0$ as $F \rightarrow 0$, but in that case it is due to the inclusion of frictional axes in the phase space. This provides the valuable insight about the hierarchy of phase space axes. Also, the method by Bagi [1] is equivalent to the uniform q model because the use of Shannon's entropy assumes a uniform DOS in the Cartesian phase space, producing the purely exponential $P_X(F_x)$. Converting this to $P_F(F)$ via Eq. (67) predicts $P_F(F) \rightarrow 0$ as $F \rightarrow 0$. However, the method is a good approximation over most of the region of experimental interest, and this indicates the importance of the layer-by-layer force conservation.

The method by Ngan [40] produces good correspondence with the empirical data in the region of weak forces, and so it predicts quite well the DOS non-uniformities in regard to weak forces without resorting to N2L or N3L. The reason for the correspondence is not yet clear, because the method is based on the energy stored in grain contacts, whereas energy stored in the packing should

not be a consideration after the non-conserving (and self-organizing) transition from the dynamic to the static regime. The explanation of this correspondence may provide an interesting alternative view of that organization.

3. Exponential Tail

This existence of the exponential tail been recently argued in Ref. (38). The exponential region of the distribution typically extends over $f > 3$ for 2D packings and $f > 2$ for 3D packings. This is seen, for example, in the qualitative difference between the 2D and 3D cases in Ref. (13). The only two cases identified thus far wherein the tail may be non-exponential over those regions are (1) packings with very few grains such that every grain is in the boundary layer [17], and (2) cases of very large grain deformation [34]. In the latter the tail $\sim \exp(-\beta f^\alpha)$ has been shown to evolve with increasing grain deformation from having an exponential form ($\alpha = 1$) to a more rapidly decaying form such as a compressed exponential ($\alpha > 1$), or perhaps a Gaussian ($\alpha = 2$). The analysis here is concerned with the rigid grain limit where the tail is exponential.

The methods by Bagi and by Kruyt and Rothenburg produce exponential tails, reflecting the fact that they maximize an entropy subject to conservation laws. The method by Ngan produces a non-exponential tail, the form of which is dependent upon the work function at the grain contacts. This does not seem correct because, in the limit of perfect rigidity with frictionless grains, packings are isostatic (so that the forces can be solved algebraically) and the geometry of the contact network becomes independent of the work function. Hence, all work functions ought to approach the same set of forces and hence the same form of the tail in the limit of perfect rigidity without friction [45]. Nevertheless, it is possible that Ngan's method with only minor adjustment might predict the correct form of the tail not only in the limit of perfect rigidity but also in the case of large deformation.

-
- [1] K. Bagi, in *Powders & Grains 97*, edited by Behringer and Jenkins (Balkema, Rotterdam, 1997), pp. 251-54; K. Bagi, *Gran. Mat.* **5**, 45 (2003).
- [2] S.F. Edwards and D.V. Grinev, *Gran. Mat.* **4**, 147 (2003).
- [3] N.P. Kruyt and L. Rothenburg, *Int. J. Solids Struct.* **39**, 571 (2002); N.P. Kruyt, *Int. J. Solids Struct.* **40**, 3537 (2003).
- [4] A.H.W. Ngan, *Phys. Rev. E* **68**, 011301 (2003).
- [5] S.J. Antony, *Phys. Rev. E* **63**, 011302 (2001).
- [6] D.L. Blair, N.W. Mueggenburg, A.H. Marshall, H.M. Jaeger, and S. R. Nagel, *Phys. Rev. E* **63**, 041304 (2001); D.M. Mueth, H.M. Jaeger, and S.R. Nagel, *Phys. Rev. E* **57**, 3164 (1998).
- [7] J.M. Erikson, N.W. Mueggenburg, H.M. Jaeger, and S.R. Nagel, *Phys. Rev. E* **66**, 040301(R) (2002).
- [8] J. Landry, G. Grest, L. Silbert, and S. Plimpton, *Phys. Rev. E* (to be published).
- [9] C.S. O'Hern, S.A. Langer, A.J. Liu, and S.R. Nagel, *Phys. Rev. Lett.* **86**, 111 (2001).
- [10] C.S. O'Hern, S.A. Langer, A.J. Liu, and S.R. Nagel, *Phys. Rev. Lett.* **88**, 075507 (2002).
- [11] F. Radjai, *Comp. Phys. Comm.* **121-122**, 294 (1999).
- [12] F. Radjai, M. Jean, J.-J. Moreau, and S. Roux, *Phys. Rev. Lett.* **77**, 274 (1996).
- [13] F. Radjai, S. Roux, and J.-J. Moreau, *Chaos* **9**, 544 (1999).
- [14] L.E. Silbert, G.S. Grest, and J.W. Landry, *Phys. Rev. E* **66**, 061303 (2002).

- [15] J.H. Snoeijer, M. van Hecke, E. Somfai, and W. van Saarloos, Phys. Rev. E **67**, 030302(R) (2003).
- [16] J.H. Snoeijer, M. van Hecke, E. Somfai, and W. van Saarloos, cond-mat/0310202 v.2 (unpublished).
- [17] J.H. Snoeijer, T.J.H. Vlugt, M. van Hecke, and W. van Saarloos, Phys. Rev. E **TBD**, to be published (2004).
- [18] C. Thornton, Kona **15**, 81 (1997).
- [19] J. Brujić, S.F. Edwards, D.V. Grinev, I. Hopkinson, D. Brujić, and H.A. Makse, Faraday Disc. **123**, 207 (2002).
- [20] A.V. Tkachenko and T.A. Witten, Phys. Rev. E **62**, 2510 (2000).
- [21] A. Mehta and S.F. Edwards, Physica A **157**, 1091 (1989); S.F. Edwards and C.C. Mounfield, Physica A **226**, 1 (1996); S.F. Edwards and D.V. Grinev, Chaos **9**, 551 (1999); S.F. Edwards and D.V. Grinev, Physica A **263**, 545 (1999); P.G. de Gennes, Rev. Mod. Phys. **71** S374 (1999); R.C. Ball and D.V. Grinev, Physica A **292**, 167 (2001); S.F. Edwards and D.V. Grinev, Physica A **294**, 57 (2001); A. Coniglio and M. Nicodemi, Physica A **296**, 451 (2001); S.F. Edwards and D.V. Grinev, Physica A **302**, 162 (2001); V. Colizza, A. Barrat, and V. Loreto, Phys. Rev. E **65**, 050301 (2002); A. Fierro, M. Nicodemi, and A. Coniglio, Phys. Rev. E **66**, 061301 (2002); R. Blumenfeld and S.F. Edwards, Phys. Rev. Lett. **90**, 114303 (2003); A. Coniglio, A. Fierro, and M. Nicodemi, cond-mat/0305175 (unpublished).
- [22] J.P. Bouchaud, cond-mat/0211196 v.2 (unpublished).
- [23] S.F. Edwards and R.B.S. Oakeshott, Physica A **157**, 1080 (1989).
- [24] J.-P. Bouchaud, P. Claudin, D. Levine, and M. Otto, Eur. Phys. J. E **4**, 451 (2001); M. Otto, J.-P. Bouchaud, P. Claudin, and J.E.S. Socolar, Phys. Rev. E **67**, 031302 (2003); J.E.S. Socolar, Discrete Cont. Dyn. B **3**, 601 (2003).
- [25] P. Claudin, J.-P. Bouchaud, M.E. Cates, and J.P. Wittmer, Phys. Rev. E **57**, 4441 (1998); A.V. Tkachenko and T.A. Witten, Phys. Rev. E **60**, 687 (1999); J. Rajchenbach, Phys. Rev. E **63**, 041301 (2001); J. Geng, D. Howell, E. Longhi, R.P. Behringer, G. Reydellet, L. Vanel, E. Clément, and S. Luding, Phys. Rev. Lett. **87**, 035506 (2001); D. Serero, G. Reydellet, P. Claudin, É. Clément, and D. Levine, Eur. Phys. J. E **6**, 169 (2001); C.F. Moukarzel, J. Phys. Cond. Mat. **14**, (2002); N.W. Mueggenburg, H.M. Jaeger, and S.R. Nagel, Phys. Rev. E **66**, 031304 (2002); L. Breton, P. Claudin, É. Clément, and J.-D. Zucker Europhys. Lett. **60**, 813 (2002); J. Geng, G. Reydellet, E. Clément, and R.P. Behringer, Physica D **182**, 274 (2003).
- [26] M.E. Cates, J.P. Wittmer, J.-P. Bouchaud, and P. Claudin, Chaos **9**, 511 (1999); E. Aharonov and D. Sparks, Phys. Rev. E **60**, 6890 (1999); E. Kolb, J. Cviklinski, J. Lanuza, P. Claudin, and E. Clément, cond-mat/0308054 (unpublished?), J.A. Drocco, M.B. Hastings, C.J. Olson Reichhardt, and C. Reichhardt, cont-mat/0310291 (unpublished).
- [27] C.S. O'Hern, L.E. Silbert, A.J. Liu and S.R. Nagel, Phys. Rev. E **68**, 011306 (2003).
- [28] C-h.Lu, S.R. Nagel, D.A. Schecter, S.N. Coppersmith, S. Majumdar, O. Narayan, and T.A. Witten, Science **269**, 513 (1995).
- [29] S.N. Coppersmith, C-h. Liu, S. Majumdar, O. Narayan, and T.A. Witten, Phys. Rev. E **53**, 4673 (1996).
- [30] R.C. Youngquist and P.T. Metzger (unpublished).
- [31] C. Eloy and E. Clément, J. Phys. I (France) (1997); E.B. Pitman, Phys. Rev. E **57**, 3170 (1998); M. Nicodemi, Phys. Rev. Lett. **80**, 1340 (1998); J.E.S. Socolar, Phys. Rev. E **57**, 3204 (1998); M.G. Sexton, J.E.S. Socolar, D.G. Schaeffer, Phys. Rev. E **60**, 1999 (1999); O. Narayan, Phys. Rev. E **63**, 010301 (2000); T. Aste, T. Di Matteo, and E.G. d'Agliano, J. Phys. Cond. Mat. **14**, 2391 (2002).
- [32] M.L. Nguyen and S.N. Coppersmith, Phys. Rev. E **59**, 5870 (1999).
- [33] M.L. Nguyen and S.N. Coppersmith, Phys. Rev. E **62**, 5248 (2000).
- [34] H.A. Makse, D.L. Johnson, and L.M. Schwartz, Phys. Rev. Lett. **84**, 4160 (2000).
- [35] E.R. Nowak, J.B. Knight, E. Ben-Naim, H.M. Jaeger, S.R. Nagel, Phys. Rev. E **57**, 1971 (1998); J.J. Brey, A. Prados, Phys. Rev. E **68**, 051302 (2003).
- [36] H. Troadec, F. Radjai, S. Roux, and J.C. Charmet, Phys. Rev. E **66**, 041305 (2002).
- [37] A.V. Tkachenko and T.A. Witten, Phys. Rev. E **60**, 687 (1999); L.E. Silbert, D. Ertaş, G.S. Grest, T.C. Halsey, and D. Levine, Phys. Rev. E **65**, 031304 (2002); A. Kasahara and H. Nakanishi, cond-mat/0312598 (2003).
- [38] P.T. Metzger, Phys. Rev. E (Comment to Ngan to be published).
- [39] H.A. Makse and J. Kurchan, Nature **415**, 614 (2002).
- [40] A.H.W. Ngan, Phys. Rev. E (Reply to Metzger to be published).
- [41] The use of the letter “w” for the loads derives from other studies where they have been called “weights”. This word has been avoided here simply because the ensemble is without gravity.
- [42] In general, whenever subscripted variables appear in an argument of a function and there is no sum or product over that subscript, it will be understood that the argument contains the entire list.
- [43] More importantly, it should be noted that $P_f(f)$ along the boundary of a container is really $P_w(w)$, and due to the unusual contact geometries in the boundary layer the form of $P_f(f)$ is not necessarily the same as it is in the bulk. These relationships were studied in Refs. (15) and (16), showing at least qualitative if not quantitative similarity between the bulk and boundary distributions. The numerical simulation studies have published values for the exponential tail decay constant allowing for a more limited quantitative comparison in the bulk. These simulations have not generally been for the case of isotropic fabric and stress nor always using frictionless, rigid grains, so comparison with the behavior of the bulk in the region of weak forces can at the present be only qualitative.
- [44] A definite integral over the singularity converges, producing a finite probability as expected, so the existence of a singularity in the probability *density* should not be construed as a problem.
- [45] Ngan's argument [40] that this produces a dilemma with regard to linear elasticity is not correct, because linear elasticity is itself an idealization in the limit of vanishing strain, and hence linearity cannot be justified except in the same limit where the form of the tail becomes invariant.